N 70 34064

NASA CR 109886

NEW MEXICO STATE UNIVERSITY

LAS CRUCES, NEW MEXICO

ADVANCED STUDY OF VIDEO SIGNAL PROCESSING IN LOW SIGNAL TO NOISE ENVIRONMENTS

By

Frank Carden
Enrique Cheng

A Quarterly Progress Report

Submitted to

NATIONAL AERONAUTICAL SPACE ADMINISTRATION
WASHINGTON, D. C.

NASA RESEARCH GRANT NGR-32-003-037

Electrical Engineering Department
Communication Research Group

February 1970 - May 1970

ENGINEERING EXPERIMENT STATION

NEW
MEXICO
STATE
UNIVERSITY
LAS CRUCES, NEW MEXICO

ADVANCED STUDY OF VIDEO SIGNAL PROCESSING IN LOW SIGNAL TO NOISE ENVIRONMENTS

By

Frank Carden
Enrique Cheng

A Quarterly Progress Report

Submitted to

NATIONAL AERONAUTICAL SPACE ADMINISTRATION
WASHINGTON, D. C.

NASA RESEARCH GRANT NGR-32-003-037

Electrical Engineering Department
Communication Research Group

February 1970 - May 1970

ENGINEERING
EXPERIMENT
STATION

ABSTRACT

MULTI-FILTER PHASE-LOCKED LOOP DEMODULATION

BY

ENRIQUE CHENG, B.S.M.E. & E.E.

Master of Science in Electrical Engineering

New Mexico State University

Las Cruces, New Mexico 1970

Dr. Wiley E. Thompson, Chairman

The carrier model and the model for the generalized multi-filter phase-locked loop are considered, and state equations for the phase model are derived. Analog computer configurations showing direct component interconnections for simulations of both carrier and phase multi-filter phase-locked loop models are also obtained.

Simulations of a low-band pass multi-filter phase-locked loop, with a single deterministic sinusoidal frequency modulated sub-carrier were performed to investigate the improvement of the low-pass

phase-locked loop due to the band-pass filter. This improvement is measured by comparing the phase error of the low-band pass multi-filter phase-locked loop with the resulting low-pass phase-locked loop when the band-pass filter is removed from the loop. The simulation was accomplished by solving the state equations for the phase model on a CDC 3300 digital computer, using the Adams-Moulton numerical integration technique, and by analog computer simulation of the carrier model showing direct component interconnections.

TABLE OF CONTENTS

LIST OF ABBREVIATIONS

LIST OF SYMBOLS

SYMBOL		Page
ζ_n	Damping ratio of second order PLL.....	7
$F_K(s)$	Transfer function of linear time-invariant filter.....	9
K_{f_K}	Filter gain.....	9
ω_{o1}	Natural frequency of BP filter of second order.....	27
ζ_{o1}	Damping ratio of BP filter of second order.....	27
AK_1	Individual BP loop gain of L-BP M-PLL.....	27
ω_{n_1}	Individual BP loop natural center frequency of L-BP M-PLL.....	28
AK_2	Individual LP loop gain of L-BP M-PLL.....	28
ω_{n_2}	Individual LP loop bandwidth of L-BP M-PLL.....	30
ζ_{n_2}	Individual damping ratio of L-BP M-PLL.....	30
ω_m	Radian frequency of modulating sine wave.....	31
$\Delta\omega$	Frequency deviation.....	31
$e_{ss\ p}$	Steady-state peak detected output of M-PLL phase model.....	42
$e_{ss\ pp}$	Steady-state peak to peak detected output of M-PLL phase model.....	42
$\phi_{e_{ss\ p}}$	Steady-state peak phase error.....	43
$\dot{\phi}_{e_{ss\ p}}$	Steady-state peak to peak frequency error.....	46

LIST OF FIGURES

CHAPTER I

INTRODUCTION

Phase-locked loop receivers* (Figure 3) are widely used in detecting narrow-band telemetry signals from satellites and satellite probes. However, common phase-locked loop low-pass design characteristically yields little or no threshold improvement over conventional FM discriminators when the mode of operation involves a format with large amounts of energy at discrete (or nearly discrete) frequencies high in the base-band. An example of this type of format is shown in Figure 1.

The demodulation of this base-band structure with the single low-pass design permits the noise over the unused band, between the narrow-band, high energy subcarrier, ω_2 and ω_1, to enter the loop (Figure 1). The efficiency of the spectrum is very poor and consequently the structure turns out to be unsuitable. Furthermore, since $\omega_2 > \omega_1$, the open-loop gain at ω_2 is much lower than the gain at low base-band frequencies. Therefore, the phase error is larger and the tracking error becomes more significant.

One solution to these problems involves the use of an additional band-pass filter in the loop in parallel with the common base-band filter. Tests carried out [1] show that the addition of band-pass feedback paths in parallel with the low-pass filter (if a large amount of energy is used at more than one discrete frequency) optimize the phase-locked loop demodulation process at the upper base-band frequencies. Namely,

---

* Hereafter referred to as PLL

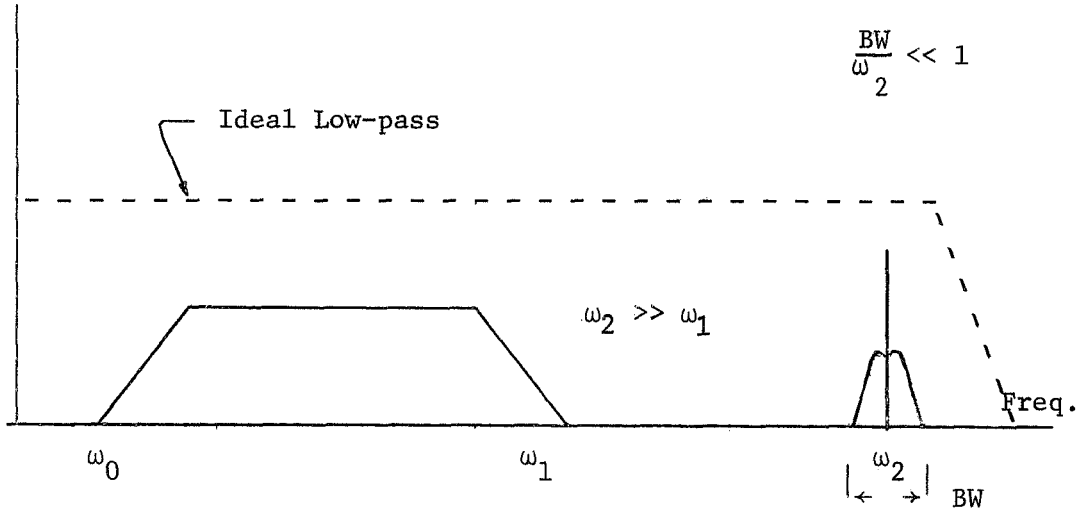

Figure 1. Frequency Spectrum Showing the Locations of a High Energy Sub-carrier at ω_2 with a Narrow-band Information

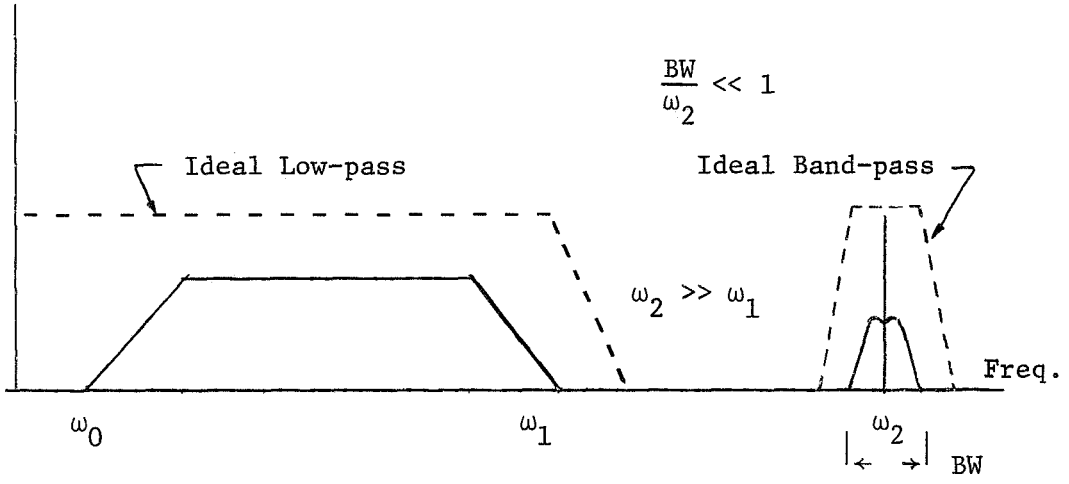

Figure 2. Illustration of the Resulting Spectrum After the Addition of the Band-pass Feedback Path and the Decrease of the Low-pass

a PLL with more than one filter in the closed-loop path, called MULTI-FILTER PLL (M-PLL), yields improvements over a standard low-pass design for this type of format (Figure 2). These evaluations were made at low frequency modulation indices and for particular conditions and parameters.

1.1 The Basic PLL

The phase-locked loop demodulator is essentially a coherent demodulator. The basic configuration for the carrier model as given by Viterbi [2] is shown in Figure 3. The Voltage-controlled oscillator (VCO) provides a constant amplitude sinusoidal signal whose instantaneous frequency varies according to the input to the VCO. The electronic multiplier and the time-invariant linear filter constitutes the phase measurement device that provides a signal error proportional to the relative phase difference between the incoming phase-modulated (PM) or frequency-modulated (FM) carrier and the locally generated clean replica of the modulated signal obtained from the VCO.

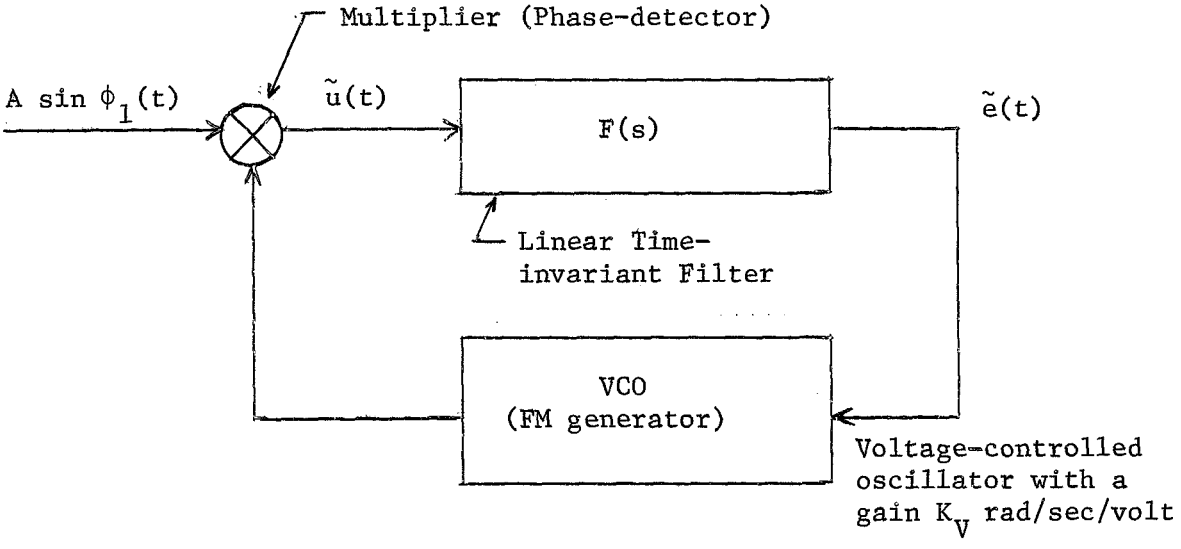

Figure 3. System Diagram for a PLL

The quantitative description of the PLL is as follows: The carrier input signal containing phase or frequency information is A sin $\phi_1(t)$, and thus the input power is $\frac{A^2}{2}$ watts. The VCO output signal is B cos $\phi_0(t)$ with a power of $\frac{B^2}{2}$ watts.

For an FM process, in the absence of noise, the instantaneous phases $\phi_1(t)$ and $\phi_0(t)$ are of the form*

$$\phi_1(t) = \omega_c t + \theta_1(t) \qquad \text{(radians)} \qquad (1.1\text{-}1)$$

$$\phi_0(t) = \omega_o t + \theta_0(t) \qquad \text{(radians)} \qquad (1.1\text{-}2)$$

where

ω_c is the carrier frequency, and

ω_o is the VCO free-running or quiescent frequency. In this thesis it is assumed $\omega_c = \omega_o$.

The variables $\theta_1(t)$ and $\theta_0(t)$ are given by

$$\theta_1(t) = K_G \int_o^t m(t)\, dt \qquad (1.1\text{-}3)$$

$$\theta_0(t) = K_V \int_o^t \tilde{e}(t)\, dt \qquad (1.1\text{-}4)$$

---

* Assuming $\phi_1(0^-) = \phi_0(0^-) = 0$

where

m(t) is the modulating information signal,

$\tilde{e}(t)$ is the filter output signal that drives the VCO and contains the information output, and

K_G and K_V are proportionality constants in rad/sec/volt.

The output $\tilde{u}(t)$ of the multiplier* is given by

$$\tilde{u}(t) = A \sin \phi_1(t) \cdot B \cos \phi_0(t) \qquad (1.1\text{-}5)$$

or

$$= \frac{AB}{2} \{\sin (\phi_1(t) - \phi_0(t)) + \sin (\phi_1(t) + \phi_0(t))\} \qquad (1.1\text{-}6)$$

Substituting equations (1.1-1) and (1.1-2) in (1.1-6), and dropping the argument t for simplicity, (1.1-6) reduces to

$$\tilde{u} = \frac{AB}{2} [\sin (\theta_1 - \theta_0) + \sin (2\omega_c t + \theta_1 + \theta_0)] \qquad (1.1\text{-}7)$$

Ordinary analysis of the loop assumes that the sum-frequency term $\frac{AB}{2} \sin (2\omega_c t + \theta_1 + \theta_0)$ is eliminated by the VCO-filter combination. And, if $\omega_c >> 1$, the assumption is still valid for cases where the linear, time-invariant filter does nothing to reject high frequencies, for example, the base-band filter $(1 + a/s)$. The validation holds because the VCO, being in essence an integrator, rejects high-frequency sinusoidals. However, in these circumstances a filter either must be put into the loop before $\tilde{e}(t)$ or it must be used on $\tilde{e}(t)$ outside of the loop to reject the sum-frequency term so that we can obtain the information-

* Assuming an ideal multiplier

modulating signal.

Therefore, the high-frequency term may be discarded from the loop analysis and (1.1-7) yields

$$\tilde{u} = \frac{AB}{2} \sin \phi_e \tag{1.1-8}$$

where

$$\phi_e \triangleq \theta_1 - \theta_0 \tag{1.1-9}$$

and its derivative

$$\dot{\phi}_e \triangleq \dot{\theta}_1 - \dot{\theta}_0 \tag{1.1-10}$$

are defined as the phase and frequency error, respectively.

The phase model configuration for this PLL is shown in Figure 4.*

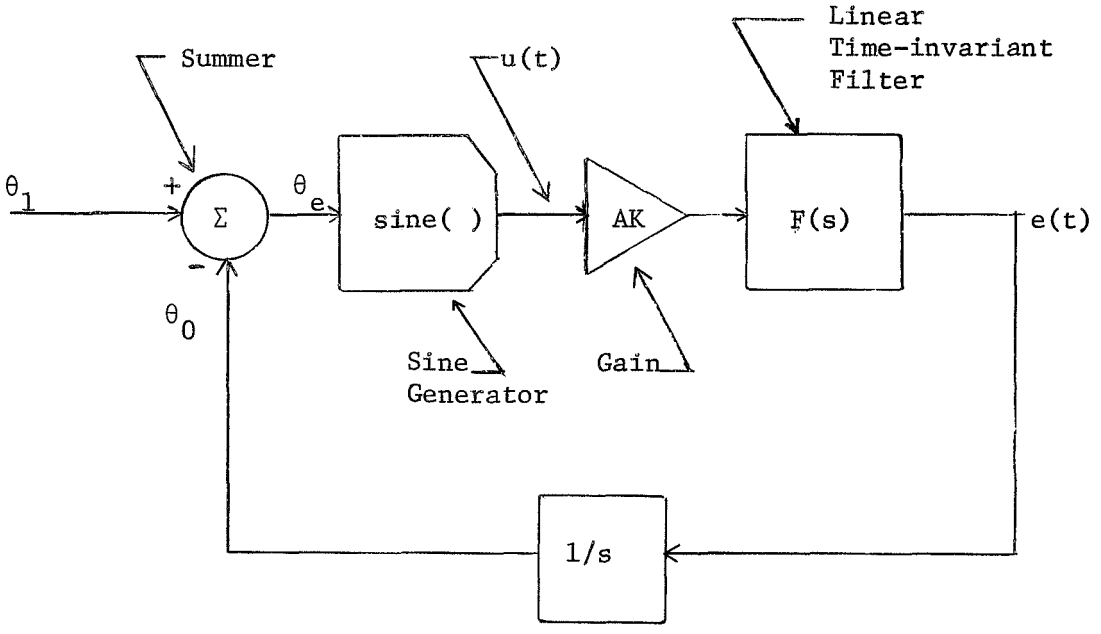

Figure 4. PLL Phase Model

* See reference [2]

where the loop-gain AK is defined as

$$AK = A(1/2)\ B\ K_V \text{ rad/sec} \tag{1.1-11}$$

One may note that the transformation from a phase-model to a carrier model is not unique.

In the more general case when the detector gain is K_δ (1.1-11) transforms to

$$AK = AK_\delta BK_V \tag{1.1-12}$$

Using the linear approximation $\sin \phi_e = \phi_e$ in the phase model, the closed-loop PLL response becomes

$$\frac{\theta_0(s)}{\theta_1(s)} = \frac{AK\ F(s)\ 1/s}{1 + AK\ F(s)\ 1/s} \tag{1.1-13}$$

For a $F(s) = 1 + a/s$

$$\frac{\theta_o(s)}{\theta_1(s)} = \frac{AK\ (s+a)}{s^2 + AKs + AKa} \tag{1.1-14}$$

Let

$$AK = 2\zeta_n \omega_n \tag{1.1-15}$$

$$AKa = \omega_n^{\ 2} \tag{1.1-16}$$

where ω_n is defined as the PLL loop bandwidth. Then (1.1-5) is a second order system of the form

$$\frac{\theta_0(s)}{\theta_1(s)} = \frac{2\zeta_n\omega_n(s + \omega_n/2\zeta_n)}{s^2 + 2\zeta_n\omega_n s + \omega_n^2} \qquad (1.1\text{-}17)$$

A sketch of the amplitude-frequency reponse of the PLL with a base-band filter (1 + a/s) is shown in Figure 5. From the figure one can see that this PLL has the characteristic of a low-pass filter from which it is usually designated as a low-pass PLL (LP PLL).

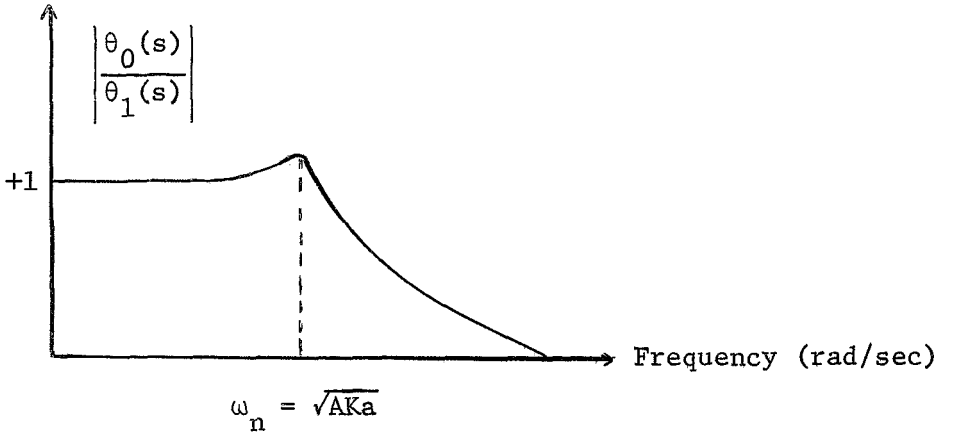

Figure 5.

Amplitude-Frequency Response of PLL with a Base-band Filter (1 + a/s)

CHAPTER II

MATHEMATICAL MODEL AND SIMULATION OF A MULTI-FILTER PLL

2.1 The M-PLL

A carrier model configuration for the generalized M-PLL is given in Figure 6a and its phase model equivalent is given in Figure 6b.

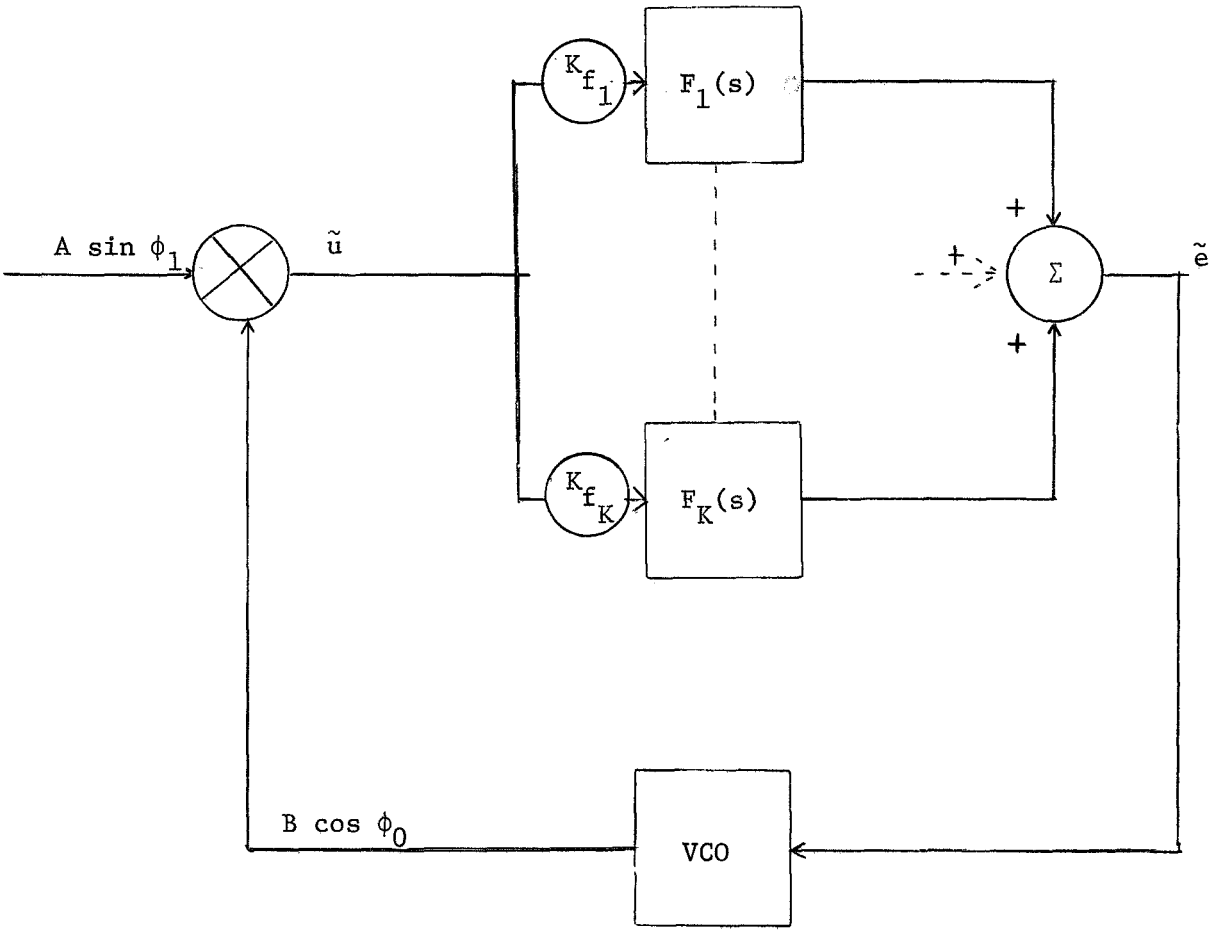

Figure 6a.
M-PLL Carrier Model

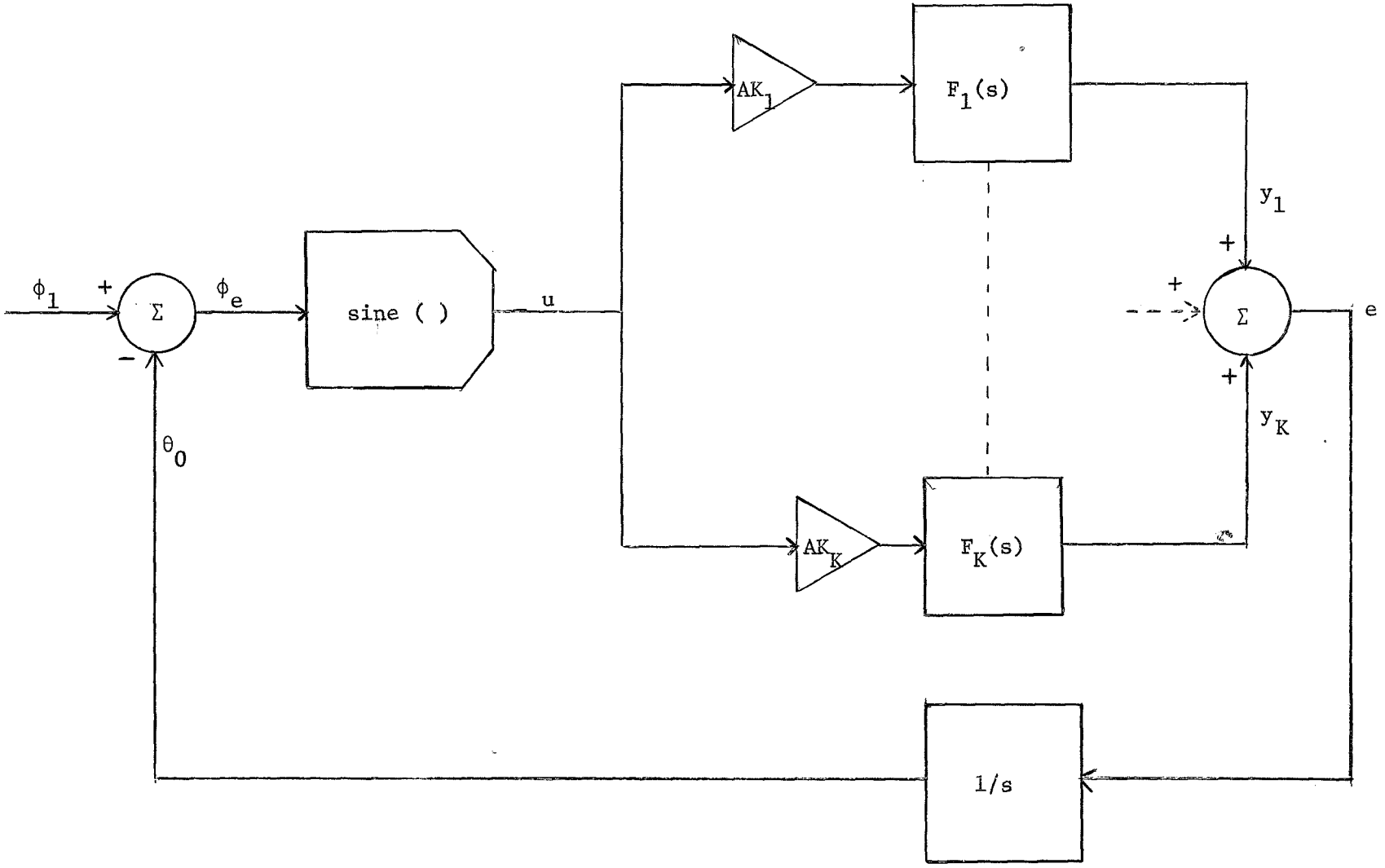

Figure 6b . M-PLL Phase Model

The transfer function for the linear model of Figure 6b is given by

$$\frac{\theta_0(s)}{\theta_1(s)} = \frac{\frac{1}{s}\sum_{1}^{K} AK_i F_i(s)}{1 + \frac{1}{s}\sum_{1}^{K} AK_i F_i(s)} \qquad i = 1,2,\ldots,K \qquad (2.1\text{-}1)$$

or

$$\frac{\theta_0(s)}{\theta_1(s)} = \frac{AK_1F_1(s)}{s + \sum_{1}^{K} AK_i F_i(s)} + \frac{AK_2F_2(s)}{s + \sum_{1}^{K} AK_i F_i(s)} + \ldots + \frac{AK_KF_K(s)}{s + \sum_{1}^{K} AK_i F_i(s)}$$

$$i = 1,2,\ldots,K \qquad (2.1\text{-}2)$$

For a suitable application of linear analysis to the multi-filter PLL it is convenient if the closed-loop response of the filters are independents. That is, if the closed-loop response at any particular frequency can be considered to be due to only one of the filters, (2.1-2) reduces to

$$\frac{\theta_0(s)}{\theta_1(s)} \cong \frac{AK_1F_1(s)}{s + AK_1F_1(s)} + \frac{AK_2F_2(s)}{s + AK_2F_2(s)} + \ldots + \frac{AK_KF_K(s)}{s + AK_KF_K(s)} \qquad (2.1\text{-}3)$$

2.2 Simulation of the M-PLL

Essentially two approaches can be taken for obtaining the solution for a M-PLL. One way is to define the M-PLL in terms of the mathematical models of its unconstrained components and the linear constraint equations imposed by the interconnection between the components. Then, this model can be solved by direct simulation on an analog computer or

by using an analog simulation program on a digital computer.

Another approach is to combine these component models and interconnection equations to obtain a reduced model - a state model - which can be solved by numerical methods on a digital computer or by simulation on an analog computer.

Solutions are obtained in this thesis by the first approach using an analog computer simulation and by the second approach using a numerical integration technique on a digital computer.

2.3 State Model for the M-PLL

A state model is derived only for the phase model because solutions of the carrier model would take more computer time. The derivation is accomplished by first obtaining state models for the components in the M-PLL and then interconnecting these component equations to obtain a model for the M-PLL.

a) Filters Component Equations - Consider a filter $F_i(s)$ whose Laplace transforms of its input and output are $u(s)AK_i$ and $Y_i(s)$ as shown in Figure 7a.

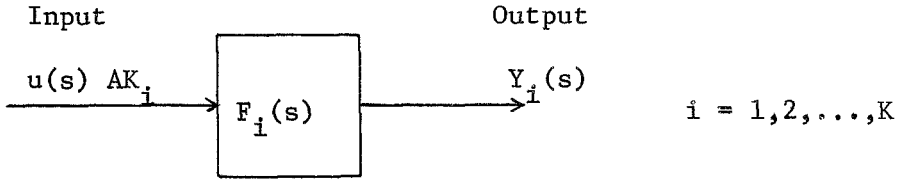

Figure 7a. Simplified Diagram of a Generalized Filter

In general $F_i(s)$ is of the form

$$F_i(s) = \frac{Y_i(s)}{u(s)AK_i} = \frac{{}^{(i)}Pm_i\, s^{m_i} + {}^{(i)}Pm_i{-}1\, S^{m_i-1} + \ldots + {}^{(i)}P_1 s + {}^{(i)}Po}{s^{n_i} + {}^{(i)}q_{n_i-1} s^{n_i-1} + \ldots + {}^{(i)}q_1\, s + {}^{(i)}q_o} = \frac{P_i(s)}{Q_i(s)} \qquad (2.3\text{-}1)$$

The filter in Figure 7a defined by (2.3-1) can be considered as two cascade filters as shown in Figure 7b.

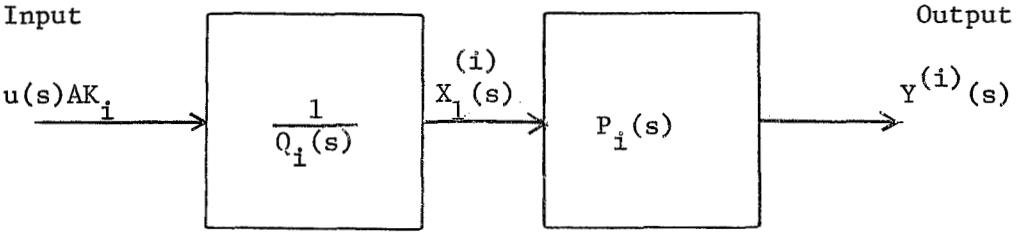

Figure 7b.
Diagram of Generalized Filter Illustrating Denominator and Numerator

where

$$Q_i(s)\ {}^{(i)}X_1(s) = u(s)AK_i \qquad (2.3\text{-}2)$$

and

$$P_i(s)\ {}^{(i)}X_1(s) = {}^{(i)}Y(s) \qquad (2.3\text{-}3)$$

or in detail

$$s^{n_i}\,{}^{(i)}X_1(s) + {}^{(i)}q_{n_i-1}\, s^{n_i-1}\,{}^{(i)}X_1(s) + \ldots + {}^{(i)}q_1\, s\,{}^{(i)}X_1(s) = u(s)\, AK_i \qquad (2.3\text{-}4)$$

and

$$P_{m_i}^{(i)} s^{m_i} X_1^{(i)}(s) + P_{m_i-1}^{(i)} s^{m_i-1} X_1^{(i)}(s) + \ldots + P_1^{(i)} s X_1^{(i)}(s) + P_o^{(i)} X_1^{(i)}(s) = Y^{(i)}(s) \qquad (2.3\text{-}5)$$

Assuming that the initial condition polynomial* is zero and taking the inverse Laplace transform of (2.3-4) and (2.3-5) we obtain**

$$\frac{d^{n_i}}{dt^{n_i}} X_1^{(i)}(t) + q_{n_i-1}^{(i)} \frac{d^{n_i-1}}{dt^{n_i-1}} X_1^{(i)}(t) + \ldots + q_0^{(i)} X_i^{(i)}(t) = u(t)\, AK_i \qquad (2.3\text{-}6)$$

$$P_{m_i}^{(i)} \frac{d^{m_i}}{dt^{m_i}} X_1^{(i)}(t) + P_{m_i-1}^{(i)} \frac{d^{m_i-1}}{dt^{m_i-1}} X_1^{(i)}(t) + \ldots + P_o^{(i)} X_i^{(i)}(t) = Y(t) \qquad (2.3\text{-}7)$$

Dropping the argument, t, for simplicity and letting

$$\dot{X}_1^{(i)} = \dot{X}_2^{(i)}, \quad \dot{X}_2^{(i)} = X_3^{(i)}, \ \ldots, \ \dot{X}_{n_i-1}^{(i)} = X_{n_i}^{(i)} \qquad (2.3\text{-}8)$$

(2.3-6 can be written as

---

* This enables us to pass from the transfer function back to the original equation.

**We merely replace $\frac{d}{dt}$ by s.

$$\frac{d}{dt}\begin{bmatrix} X_1^{(i)} \\ X_2^{(i)} \\ \cdot \\ \cdot \\ \cdot \\ X_{n_i}^{(i)} \end{bmatrix} = \begin{bmatrix} 0 & 1 & & & \\ 0 & 0 & 1 & & \\ & & & & \\ & & & & \\ 0 & & & 0 & 1 \\ -q_0^{(i)} & -q_1^{(i)} & \cdots & & q_{n_i-1}^{(i)} \end{bmatrix} \begin{bmatrix} X_1^{(i)} \\ X_2^{(i)} \\ \cdot \\ \cdot \\ \cdot \\ X_{n_i}^{(i)} \end{bmatrix} + \begin{bmatrix} 0 \\ 0 \\ \cdot \\ \cdot \\ 0 \\ AK_i \end{bmatrix} u \qquad (2.3\text{-}9)$$

and (2.3-7) as

$$y^{(i)} = p_0^{(i)} X_1^{(i)} + p_1^{(i)} X_2^{(i)} + \cdots + p_{m_i-1}^{(i)} X_{m_i}^{(i)} + p_{m_i}^{(i)} X_{m_i+1}^{(i)} \qquad (2.3\text{-}10)$$

If $m_i = n_i$ then

$$X_{m_i+1}^{(i)} = -q_0^{(i)} X_1^{(i)} - q_1^{(i)} X_2^{(i)} \cdots - q_{n_i-1}^{(i)} X_{n_i}^{(i)} + AK_i \qquad (2.3\text{-}11)$$

and (2.3-10) becomes

$$y^{(i)} = (p_0^{(i)} - p_{n_i}^{(i)} q_0^{(i)}) X_1^{(i)} + (p_1^{(i)} - p_{n_i}^{(i)} q_1^{(i)}) X_2^{(i)} + \cdots$$

$$+ (p_{n_i-1}^{(i)} - p_{n_i}^{(i)} q_{n_i-1}^{(i)}) X_{n_i}^{(i)} + p_{n_i}^{(i)} AK_i u \qquad (2.3\text{-}12)$$

In general

$$Y^{(i)} = [(p_0^{(i)} - p_{n_i}^{(i)} q_0^{(i)})(p_1^{(i)} - p_{n_i}^{(i)} q_1^{(i)}) \ \ldots$$

$$\ldots(p_{n_i-1}^{(i)} - p_{n_i}^{(i)} q_{n_i-1}^{(i)})] \begin{bmatrix} x_1^{(i)} \\ x_2^{(i)} \\ \cdot \\ \cdot \\ \cdot \\ x_{n_i}^{(i)} \end{bmatrix} + p_{n_i} A K_i u \qquad (2.3\text{-}13)$$

where $p_J^{(i)} = 0$ for $J > m_i$.

b) Voltage-controlled Oscillator

The VCO in the phase model is represented by an integrator. Its simplified diagram is shown in Figure 8.

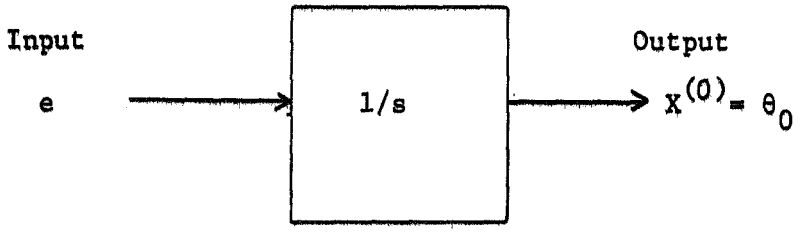

Figure 8. VCO Simplified Diagram

Then $$\dot{\theta}_0 = e \tag{2.3-14}$$

and letting $X^{(0)} = \theta$ we have $$\dot{X}^{(0)} = e \tag{2.3-15}$$

Interconnecting the component equations in accordance with the component interconnections as shown in Figure 6b, we obtain the final state model (2.3-18). System variables such as the detected output and the phase error are given by

$$e(t) = y^{(1)} + \ldots + y^{(K)} \tag{2.3-16}$$

$$\phi_e = (\theta_1 - X^{(0)}) \tag{2.3-17}$$

$$\frac{d}{dt}\begin{bmatrix} X_1^{(1)} \\ \cdot \\ \cdot \\ X_{n_1}^{(1)} \\ \cdot \\ \cdot \\ \cdot \\ X_1^{(K)} \\ \cdot \\ \cdot \\ X_{n_K}^{(K)} \\ X^{(0)} \end{bmatrix} = \tag{2.3-18}$$

Filter 1 (rows $X_1^{(1)}$ through $X_{n_1}^{(1)}$)

Filter K (rows $X_1^{(K)}$ through $X_{n_K}^{(K)}$)

VCO (row $X^{(0)}$)

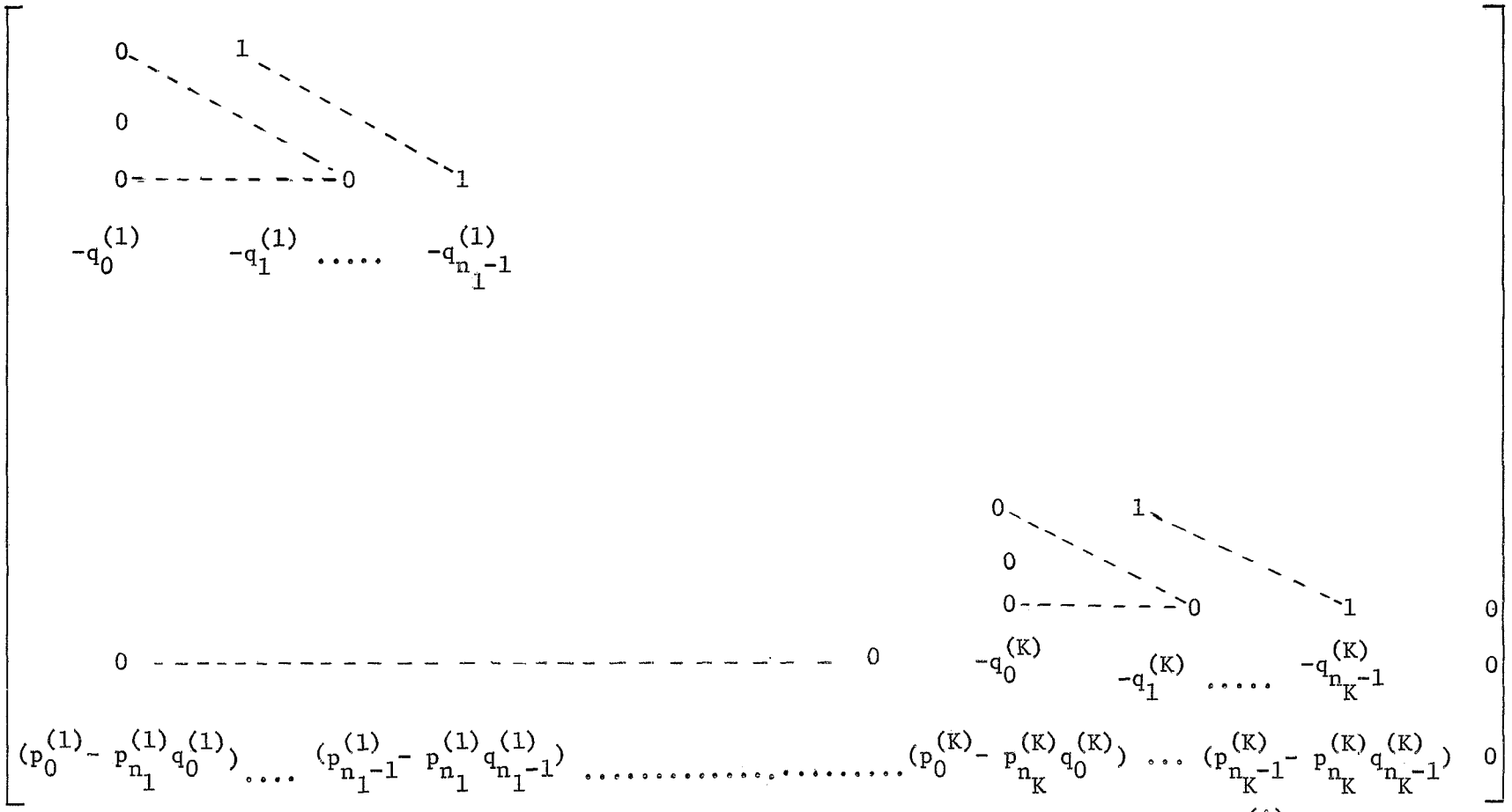

(2.3-18) State Variable Differential Equation for the M-PLL Phase Model (where $p_J^{(i)} = 0$ for $J > m_i$)

$$\begin{bmatrix} X_1^{(1)} \\ \cdot \\ \cdot \\ X_{n_1}^{(1)} \\ \cdot \\ \cdot \\ \cdot \\ X_1^{(K)} \\ \cdot \\ \cdot \\ X_{n_K}^{(K)} \\ X^{(0)} \end{bmatrix} + \begin{bmatrix} 0 \\ \cdot \\ \cdot \\ AK_1 \sin(\theta_1 - X^{(0)}) \\ \cdot \\ \cdot \\ \cdot \\ 0 \\ \cdot \\ \cdot \\ AK_K \sin(\theta_1 - X^{(0)}) \\ (p_{n_1}^{(1)} AK_1 + p_{n_2}^{(2)} AK_2 + \ldots + p_{n_K}^{(K)} AK_K) \sin(\theta_1 - X^0) \end{bmatrix} \quad (2.3\text{-}18)$$

State Variable Differential Equation For The M-PLL Phase Model

Where $p_J^{(i)} = 0$ for $J > m_i$

As previously mentioned, the solution of (2.3-18) was obtained by numerical integration on a digital computer. In particular, a subroutine based on the familiar Adams-Moulton integrating technique was used. The FORTRAN program was prepared for a CDC-3300 computer, and plots of the states and other system variables were obtained.

2.4 Analog Computer System Configuration of the M-PLL Direct Component Interconnections

Although (2.3-18) could be solved by analog simulation, the component interconnections shown in Figure 6a and Figure 6b were simulated directly on the analog computer.*

The analog computer system configuration for the M-PLL phase model is shown in Figure 9. The main problem with this model is that for high input level $\dot{\phi}_e$, the output sin ϕ_e of the sine function generator tends to increase beyond its theoretical boundary of one unit. Attempts were made to compensate for this increase but no success was obtained.

A version of the analog computer PLL carrier model** for the multi-filter PLL is given in Figure 10a. One may consider the VCO in the carrier model as being a mapping of the sine generator in the phase model. In the carrier model (C. M.) the growth of the VCO output can directly be compensated for without danger of altering the results. This is because the frequency of the VCO rather than its amplitude is a system variable.

The inconvenience with this model is that the phase error does not appear explicitly in the loop and can only be obtained explicitly thru an open loop integrator (integrator 3-11 in Figure 10a). Nevertheless, the determination of the phase error becomes quite simple if the oscilloscope is used to observe sin ϕ_e vs ϕ_e*** (Figure 10c).

---

* TR-20 EIA analog computers were used.

** For detailed information about the analog computer PLL carrier refer to [3].

*** sin ϕ_e is obtained from amplifier no. 3 in Figure 10a after filtering out the sum-frequency term.

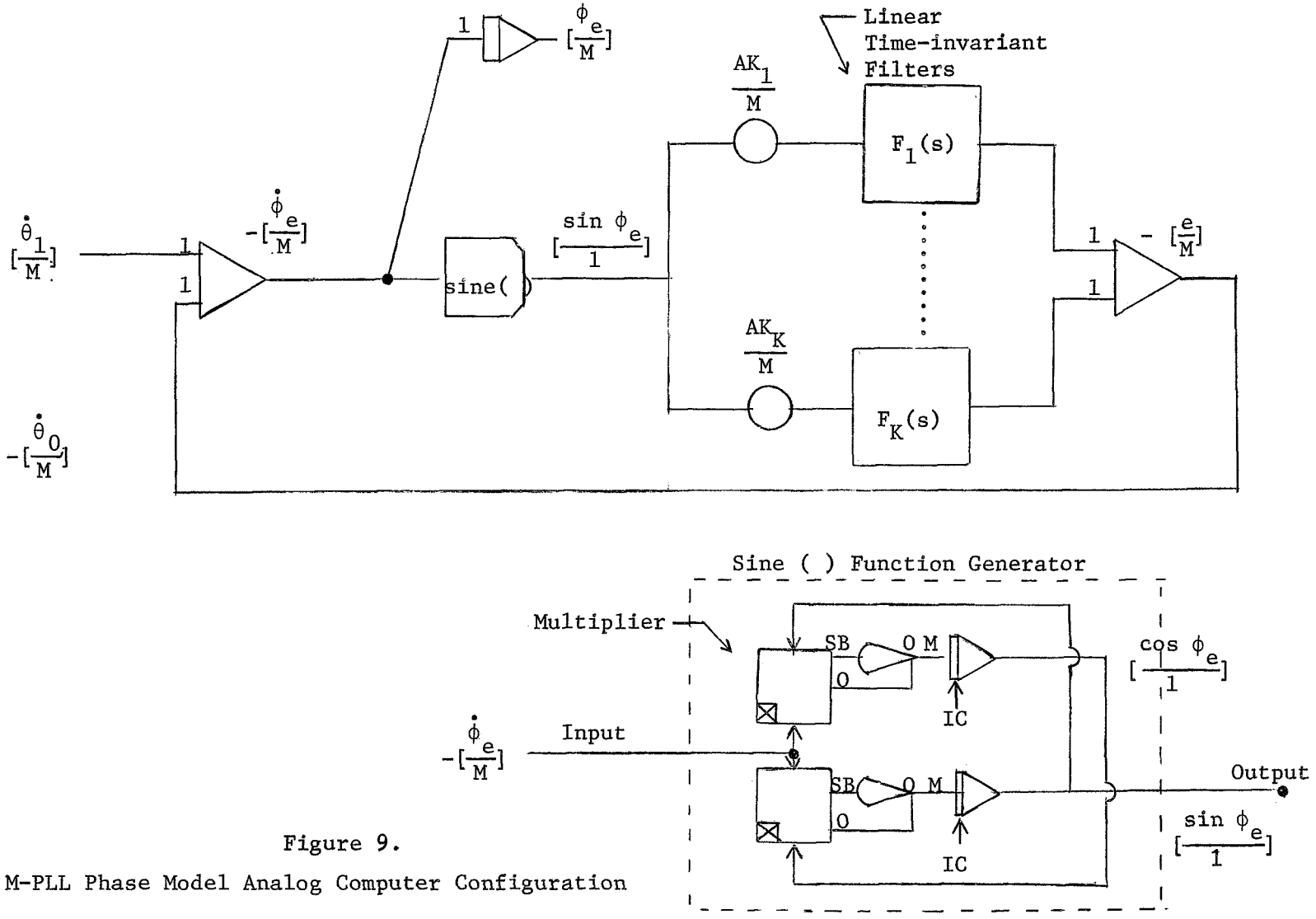

Figure 9.

M-PLL Phase Model Analog Computer Configuration

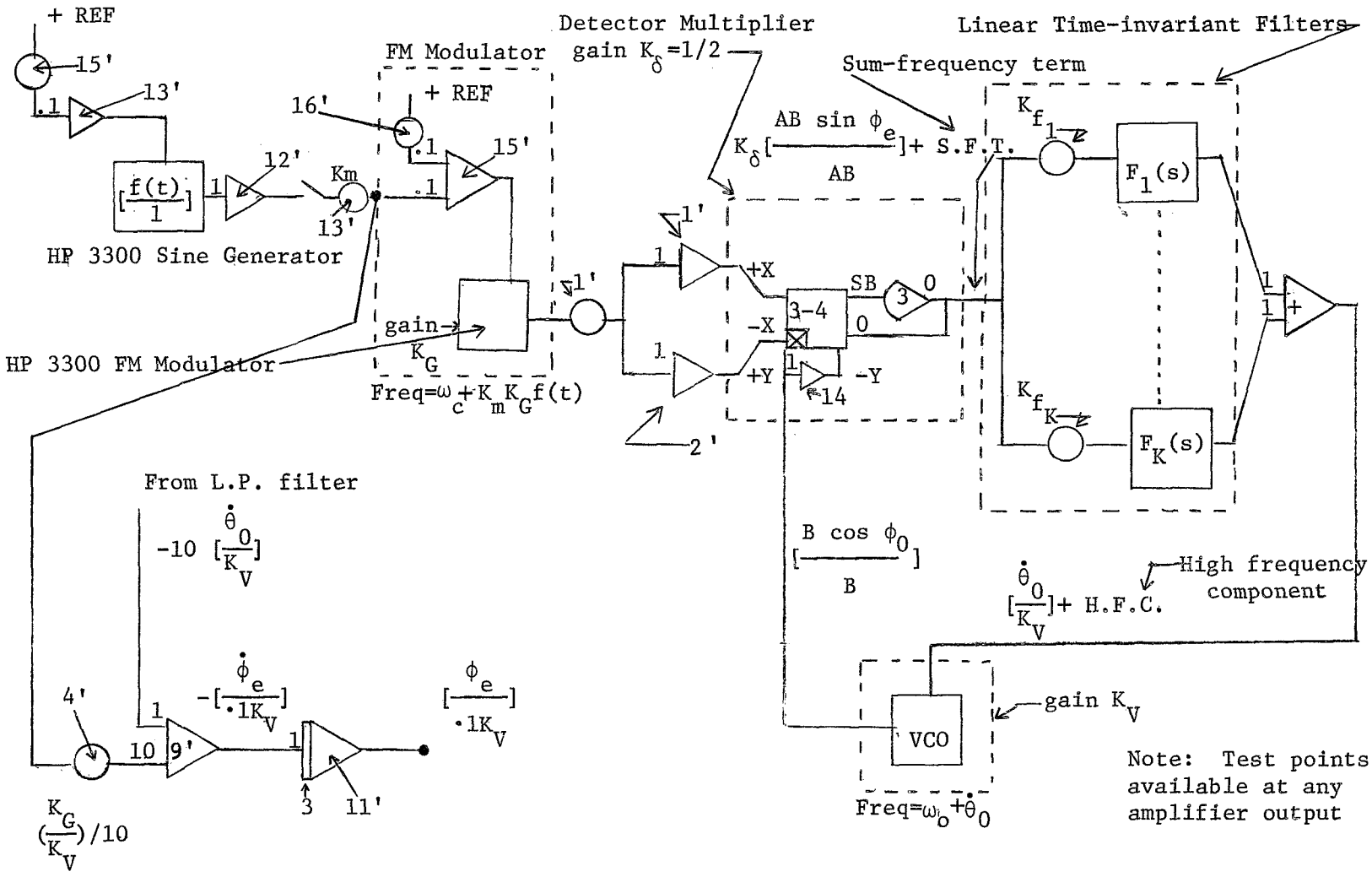

Figure 10a. M-PLL Carrier Model Analog Computer Configuration

Pot 13' sets the FM modulator index.

Pot 15' and amplifier 13' set the frequency of the information signal f(t).

Amplifier 12' isolates the output of generator $[\frac{f(t)}{1}]$.

Pot 16' sets the carrier frequency ω_c.

Pot 1' controls the output signal of the FM modulator.

Amplifiers 1' and 2' isolate the output of the FM modulator.

K_G is the HP 3300 FM modulator gain rad/sec/unit.

K_δ is the detector multiplier gain = 0.5/volts.

K_f is the filter gain 1/unit.

K_V is the VCO gain rad/sec/unit.

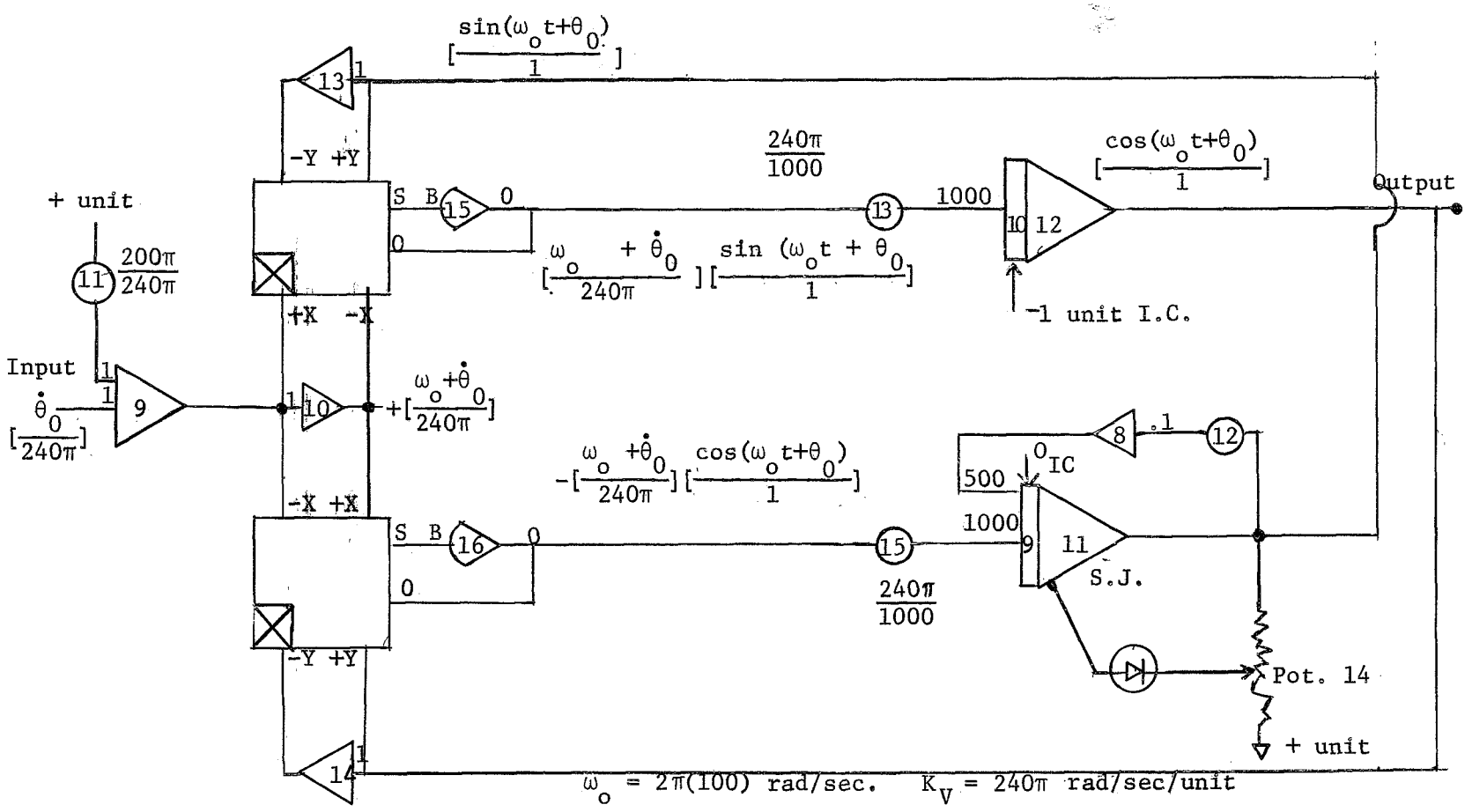

Figure 10b. VCO Analog Computer Configuration Set-up

Note:
Pot. 12 and amplifier no.8 provide positive feedback in order to prevent the output signal from decaying
Pot. 14 and semiconductor diode are the limiting elements to set the output at a fixed value

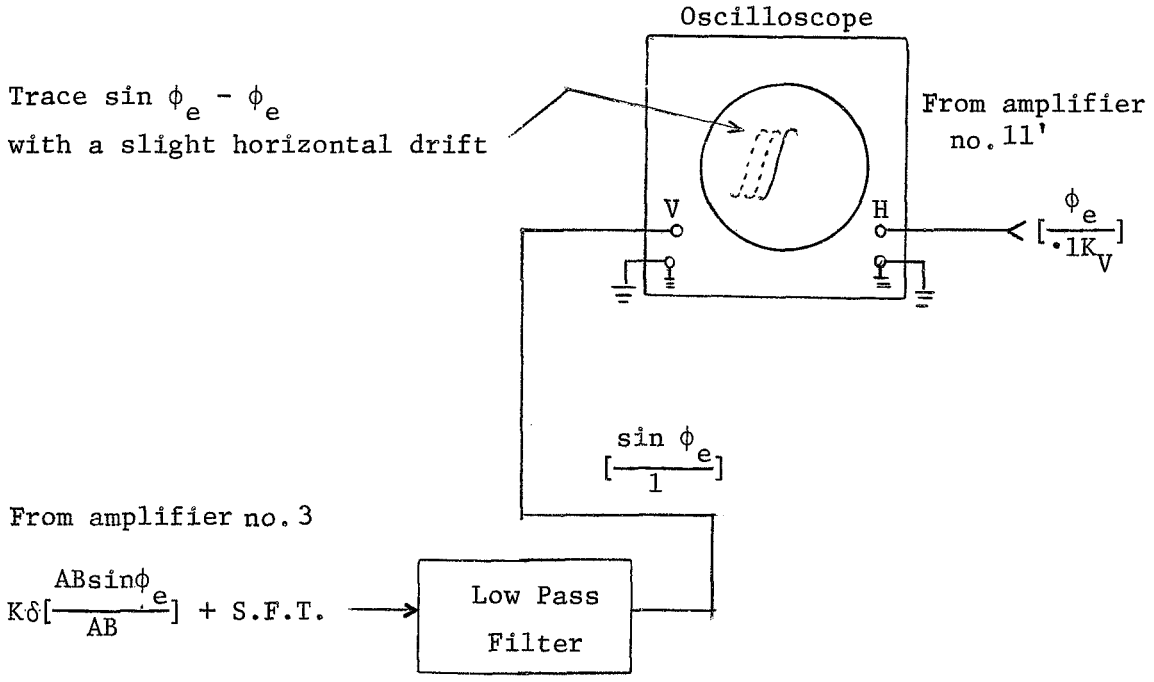

Figure 10c. System Diagram for Observation of sin ϕ_e vs. ϕ_e

CHAPTER III
SOME SIMULATIONS AND RESULTS

In this chapter, the simulation of the M-PLL with a base-band filter in parallel with a band-pass (BP) filter is considered. The base-band filter is put in the loop in carrier models in order to enable the carrier to be tracked. It is assumed that the M-PLL is initially locked onto the carrier and that a single sinusoidal deterministic sub-carrier in the frequency range of the band-pass is applied at $t = 0^{+}$.

The error signals are observed and compared with those obtained when the BP filter is removed from the loop. On the basis of this comparison the improvements introduced by the addition of the BP filter in the loop is observed, and plots of the results are presented.

3.1 A M-PLL with a Base-band and One Band-pass Filter

Let us consider a base-band filter with a transfer function given by (3.1-1) and the tuned-loop filter shown in Figure 11.

$$F_2(s) = 1 + \frac{a}{s} \tag{3.1-1}$$

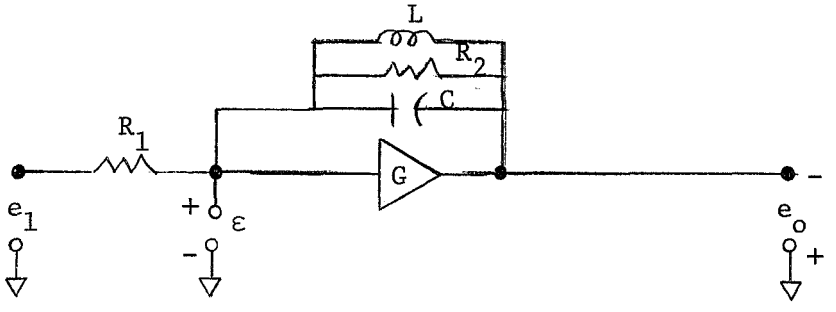

Figure 11. Tuned-loop Filter

The transfer function for the tuned-loop filter shown in Figure 11, assuming ε at virtual ground is given by

$$\frac{E_o(s)}{E_1(s)} = \bar{F}_1(s) = \frac{\frac{1}{R_1}s}{(s^2+\frac{1}{R_2C}s+\frac{1}{LC})} = \frac{K_{f_1}s}{s^2+2\zeta_{o1}\omega_{o1}s+\omega_{o1}^2} \qquad (3.1\text{-}2)$$

Then we may define a simple tuned-loop filter as

$$F_1(s) = \frac{s}{s^2 + 2\zeta_{o1}\omega_{o1}s+\omega_{o1}^2} \qquad (3.1\text{-}3)$$

For $|\phi_e|$ very small the approximation $\sin\phi_e \tilde{\simeq} \phi_e$ is quite accurate*; therefore, it is reasonable to expect that, in these circumstances, the M-PLL behavior is very well predicted by the resulting M-PLL linear phase model when the $\sin\phi_e$ element is replaced by ϕ_e in the M-PLL nonlinear phase model. For this reason, a brief analysis of the linear approximation concerning stability is presented.

Assuming that the condition for the validity of (2.1-3) is satisfied, the portion of the M-PLL open-loop transfer gain related to the tuned-loop filter (3.1-3) is given by

$$AK_1F_1(s)\frac{1}{s} = \frac{AK_1}{s^2 + 2\zeta_{o1}\omega_{o1}s + \omega_{o1}^2} \qquad (3.1\text{-}4)$$

It has only two complex conjugate poles in the LH s-plane. One can see that the system is stable for any value of the individual open-loop gain AK_1. A sketch of the root locus plot is given in Figure 12a. In an analogous manner the root locus plot for the portion corresponding to the base-band filter (3.1-1) is obtained and shown

* For $|\phi_e| < 30°$ the approximation is accurate to within 3 percent.

in Figure 12b. One can see that the individual open-loop AK_2 can reach any value without making the linear system unstable.

If a filter of the form $1/(s^2 + 2\zeta_{o1}\omega_{o1}s + \omega_{o1}^2)$ had been considered instead of (3-1-3), a bounded individual open-loop gain AK_1' would have been obtained as can be seen in the corresponding root locus plot shown in Figure 12c. Since this placed a rather large limitation in the starting analysis the filter was rejected.

The individual closed-loop response for (3.1-3) is found to be

$$\frac{\theta_0(s)}{\theta_1(s)} = \frac{AK_1 \dfrac{s}{s^2 + 2\zeta_{o1}\omega_{o1}s + \omega_{o1}^2}}{s + AK_1 \dfrac{s}{s^2 + 2\zeta_{o1}\omega_{o1}s + \omega_{o1}^2}} = \frac{AK_1}{s^2 + 2\zeta_{o1}\omega_{o1}s + \omega_{o1}^2 + AK_1} \qquad (3.1\text{-}5)$$

From (3.1-5), the individual "band-pass" loop center frequency ω_{n_1} is defined as

$$\omega_{n_1} = (\omega_{o1}^2 + AK_1)^{1/2} \qquad (3.1\text{-}6)$$

As one can see, (3.1-5) does not yield a very good BP spectrum shape. Furthermore, the maximum peak frequency in (3.1-5) differs from the maximum peak frequency of the filter (3.1-3) by an additive amount equal to the open-loop gain AK_1.

The individual closed-loop response for the base-band filter is the same as (1.1-14) but with AK_2 instead of AK. The individual LP

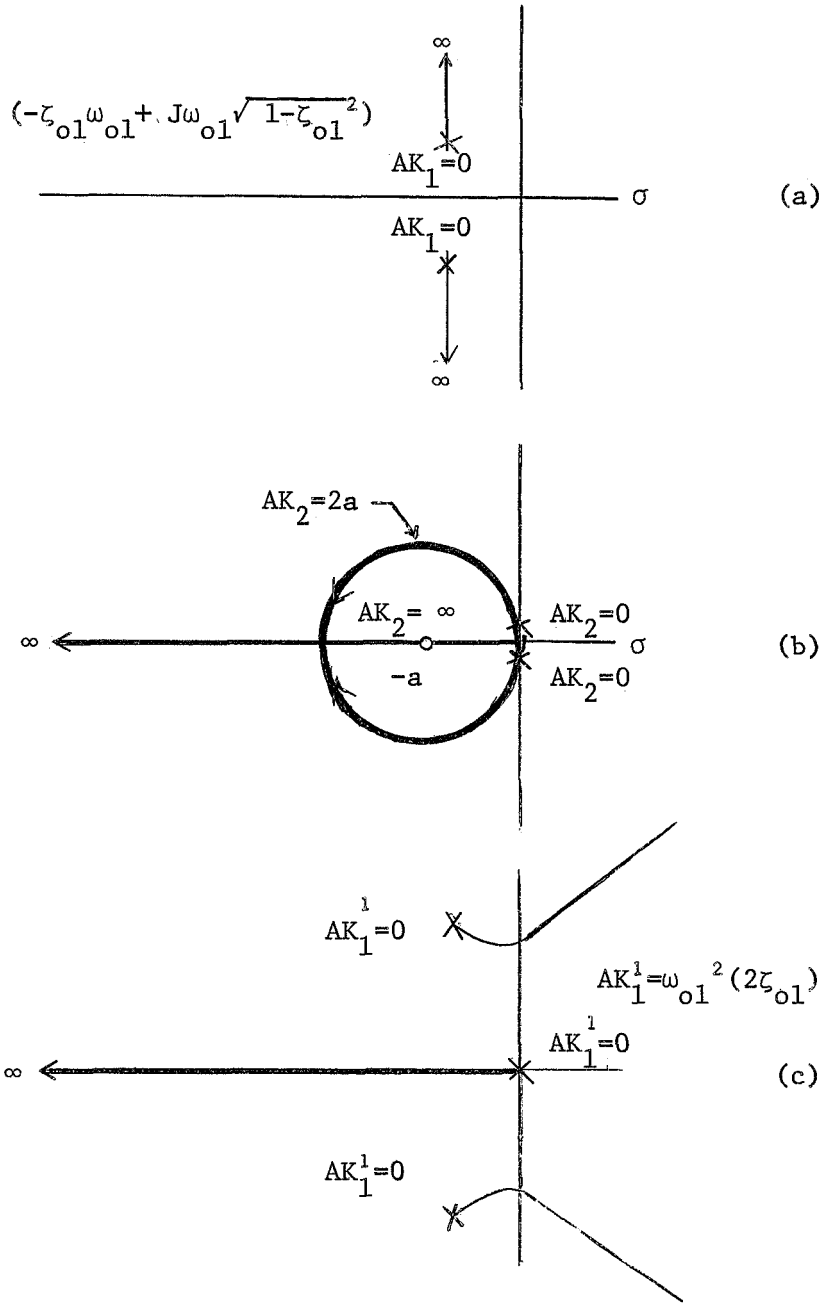

Figure 12. Root Loci for Portions of M-PLL Open-loop Transfer Gain:

(a) $AK_1F_1(s)\ 1/s = AK_1/(s^2 + 2\zeta_{o1}\omega_{o1}s + \omega_{o1}^2)$

(b) $AK_2\ F_2(s)\ 1/s = AK_2\ (1 + a/s)\ 1/s$

(c) $AK_1^1\ F_1(s)\ 1/s = AK_1^1/s\ (s^2 + 2\zeta_{o1}\omega_{o1}s + \omega_{o1}^2)$

loop bandwidth ω_{n_2} and LP loop damping ratio ζ_{n_2} are defined exactly as in an (1.1-15) and (1.1-16) where we merely replace AK_2 by AK.

From (1.1-17), (3.1-5), and (2.1-3) one can see that the closed-loop poles for the L-BP M-PLL phase model considered are fixed. This as a result of the linear approximation used since it yields constant individual closed-loop gains. In the nonlinear L-BP M-PLL phase model the equivalent individual closed-loop gains are not constants because of the nonlinear element $\sin \phi_e$. Therefore, the M-PLL closed-loop poles become variables in the s-plane.

3.1.1 Design and Simulation of the Loop

Let us first determine the state equations for the low and band-pass M-PLL (L-BP M-PLL) phase model, then the analog computer set-up for the L-BP M-PLL carrier model, and finally the values of the parameters needed to obtain the solutions on the digital computer and on the analog computer.

The state equations for the L-BP M-PLL are obtained by substituting filters (3.1-1) and (3.1-3) in the general state model (2.3-18). Thus, one obtains

$$\frac{d}{dt}\begin{bmatrix} X_1^{(1)} \\ X_2^{(1)} \\ X_1^{(2)} \\ X^{(0)} \end{bmatrix} = \begin{bmatrix} 0 & 1 & 0 & 0 \\ -\omega_{o1}^2 & -2\zeta_{o1}\omega_{o1} & 0 & 0 \\ 0 & 0 & 0 & 0 \\ 0 & 1 & a & 0 \end{bmatrix} \begin{bmatrix} X_1^{(1)} \\ X_2^{(1)} \\ X_1^{(2)} \\ X^{(0)} \end{bmatrix} + \begin{bmatrix} 0 \\ AK_1 \sin (\theta_1 - X^{(0)}) \\ AK_2 \sin (\theta_1 - X^{(0)}) \\ AK_2 \sin (\theta_1 - X^{(0)}) \end{bmatrix} \qquad (3.1.1\text{-}1)$$

To determine the initial vector [X(0+)], we assume that the PLL is initially locked onto the carrier. Then for $t < 0$

$$\theta_1 = 0 \tag{3.1.1-2}$$

$$\theta_0 = 0 \tag{3.1.1-3}$$

$$\phi_e = 0 \tag{3.1.1-4}$$

$$u = 0 \tag{3.1.1-5}$$

At $t = 0^+$, the frequency modulation is turned on. Assuming that the phase input θ_1 is of the form

$$\theta_1 = \frac{\Delta\omega}{\omega_m} \sin \omega_m t, \quad t \geq 0 \tag{3.1.1-6}$$

$$= 0 \quad , \quad t < 0$$

we have

$$\theta_0(0^-) = \theta_0(0^+) = 0 \tag{3.1.1-7}$$

since the VCO, being in essence an integrator, cannot change instantaneously.

Then

$$\theta_1(0^+) = \frac{\Delta\omega}{\omega_m} \sin (\omega_m(0)) = 0 \tag{3.1.1-8}$$

and

$$\phi_e(0^+) = \theta_1(0^+) - \theta_0(0^+) = 0 \tag{3.1.1-9}$$

$$u(0^+) = \sin \phi_e(0^+) = 0 \tag{3.1.1-10}$$

Consequently, for the initial state vector we get

$$\begin{bmatrix} X_1^{(1)} \\ X_2^{(1)} \\ X_1^{(2)} \\ X^{(0)} \end{bmatrix}_{t=0^+} = \begin{bmatrix} 0 \\ 0 \\ 0 \\ 0 \end{bmatrix} \tag{3.1.1-11}$$

System variables such as ϕ_e, e, are obtained as algebraic functions of the states. That is, from (2.3-17) we have

$$\phi_e = \theta_1 - X^{(0)} \tag{3.1.1-12}$$

and from (2.3-16) and (3.1.1-1)

$$e = X_2^{(1)} + aX_1^{(2)} + AK_2 \sin (\theta_1 - X^{(0)}) \tag{3.1.1-13}$$

Similarly, for the PLL with only the low-pass filter (LP PLL) we have

$$\frac{d}{dt} \begin{bmatrix} X_1^{(1)} \\ \underline{X}^{(0)} \end{bmatrix} = \begin{bmatrix} 0 & 0 \\ a & 0 \end{bmatrix} \begin{bmatrix} X_1^{(1)} \\ \underline{X}^{(0)} \end{bmatrix} + \begin{bmatrix} AK_2 \sin (\theta_1 - X^{(0)}) \\ \underline{AK_2} \sin (\theta_1 - X^{(0)}) \end{bmatrix} \tag{3.1.1-14}$$

with

$$\begin{bmatrix} X_1^{(1)} \\ \underline{X}^{(0)} \end{bmatrix}_{t=0^+} = \begin{bmatrix} 0 \\ 0 \end{bmatrix} \tag{3.1.1-15}$$

$$\phi_e = \theta_1 - X^{(0)} \tag{3.1.1-16}$$

$$e = aX_1^{(1)} + AK_2 (\sin \theta_1 - X^{(0)}) \tag{3.1.1-17}$$

The analog computer set-up for the L-BP M-PLL is obtained by interconnecting the analog simulators of (3.1-1) and (3.1-2) in the generalized M-PLL carrier model, shown in Figure 10a.

For the band-pass filter (3.1-3) we have

$$K_{f_1} \cdot F_1(s) = \frac{K_{f_1} s}{s^2 + 2\zeta_{o1}\omega_{o1}s + \omega_{o1}^2} = \frac{K_{f_1} s^{-1}}{1 + 2\zeta_{o1}\omega_{o1}s^{-1} + \omega_{o1}s^{-2}} = \frac{\tilde{E}_1(s)}{\tilde{U}(s)} \qquad (3.1.1\text{-}18)$$

Application of Mason's rule to (3.1.1-18) yields the signal flow graph shown in Figure 13.

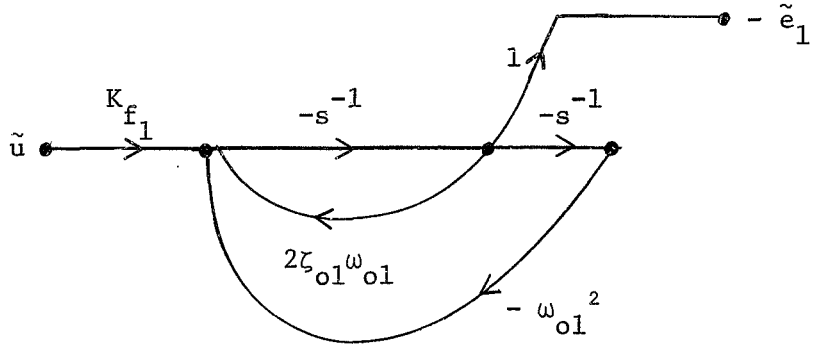

Figure 13 . Signal Flow Graph for $K_{f_1} s/(s^2 + 2\zeta_{o1}\omega_{o1}s + \omega_{o1}^2)$

Then, the analog computer set-up takes the form shown in Figure 14.

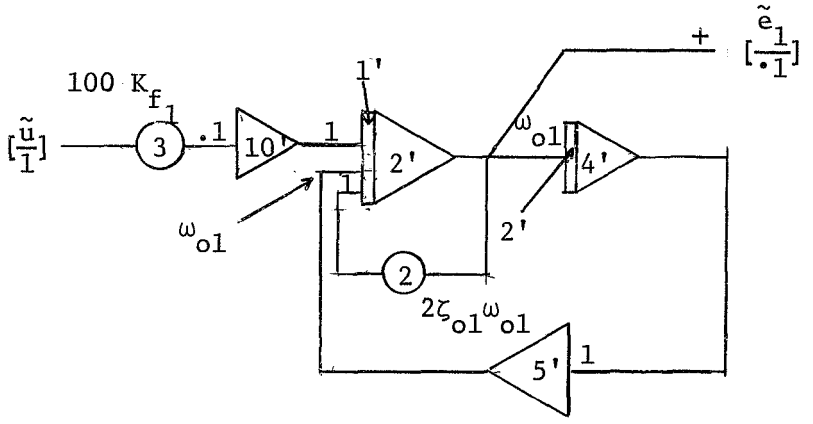

Figure 14 . Analog Computer Set-up for $K_{f_1} s/(s^2 + 2\zeta_{o1}\omega_{o1}s + \omega_{o1}^2)$

Similarly, for the base-band filter $K_{f_2} F_2(s) = K_{f_2}(1 + a/s) = \frac{\tilde{E}_2(s)}{\tilde{U}(s)}$ we get the computer set-up shown in Figure 15.

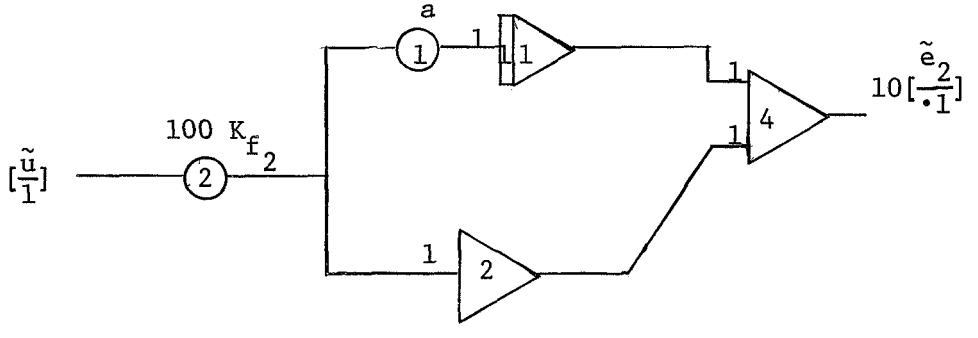

Figure 15 . Analog Computer Set-up for $K_{f_2} F_2(s) = K_{f_2}(1 + a/s)$

In determining the values of the parameters needed to perform the simulation, we recall that in section 3.1 the values of ω_{n_2}, ω_{n_1}, ζ_{n_2} could be chosen freely. However, since superposition of the individual LP and BP closed-loop responses require no interference, the loop bandwidth, ω_{n_2}, of the LP and the BP center frequency, ω_{n_1}, were set far apart.

For the LP PLL let

$$\omega_{n_2} = 1 \text{ rad / sec} \qquad (3.1.1\text{-}19)$$

$$\zeta_{n_2} = 1/\sqrt{2} \qquad (3.1.1\text{-}20)$$

and for the BP PLL let

$$\omega_{o1} = 10\ \omega_{n_2} \qquad (3.1.1\text{-}21)$$

Choose $\zeta_{o1} = 0.010 \qquad (3.1.1\text{-}22)$

so that the bandwidth of the BP filter is narrow.

Figures 16 a, b show a L-BP M-PLL phase magnitude response for the linear approximation, for values of ω_{n_2}, ζ_{n_2}, ω_{o_1}, ζ_{o_1}, given above when $AK_1 = AK_2 = \sqrt{2}$.

From equations (1.1-15) and (1.1-16)

$$AK_2 = 2\zeta_{n_2}\omega_{n_2} = 2\ (\ 1/\sqrt{2})\ (1) = \sqrt{2} \qquad (3.1.1\text{-}23)$$

$$AK_2a = \omega_{n_2}^2 = (1)^2 = 1 \qquad (3.1.1\text{-}24)$$

If A = B = 1, then

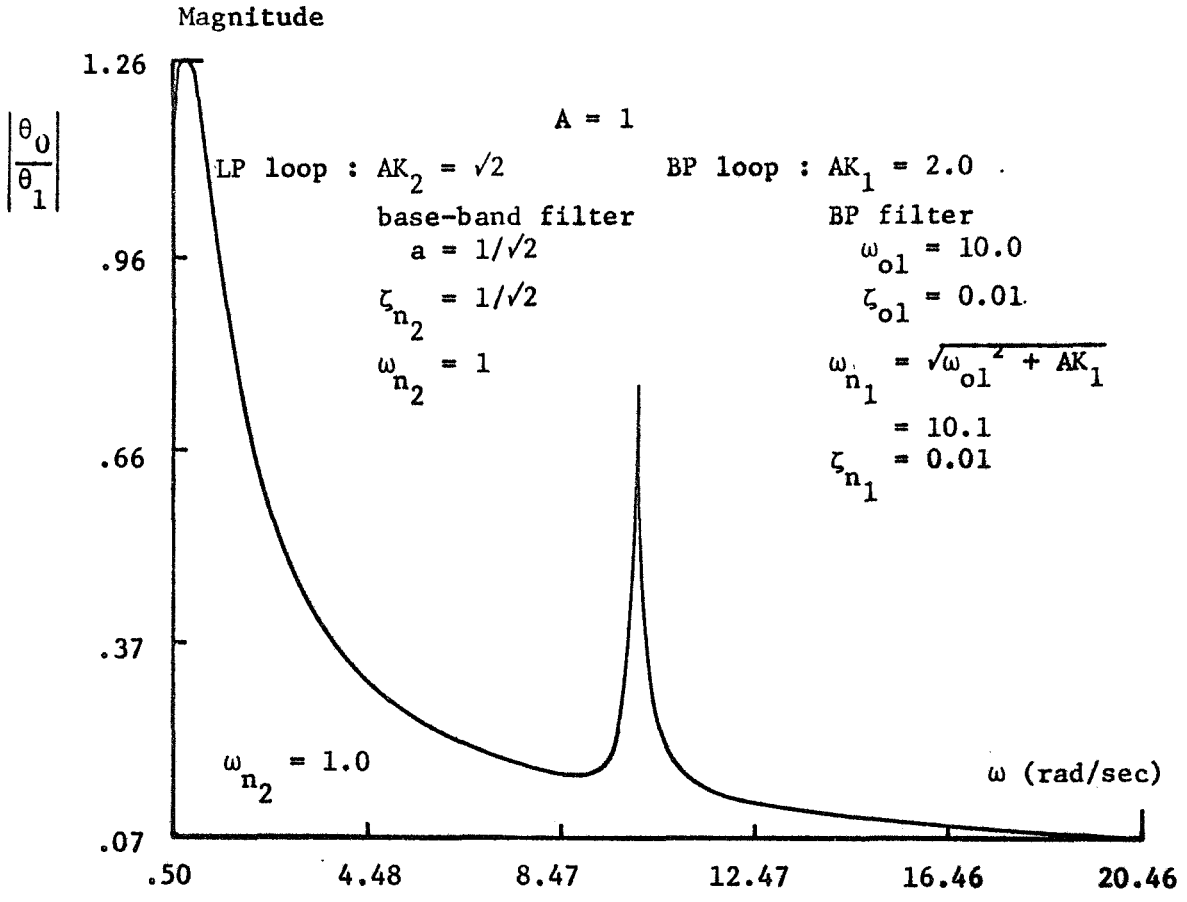

Figure 16a. L-BP M-PLL Phase Magnitude Response for the Linear Approximation

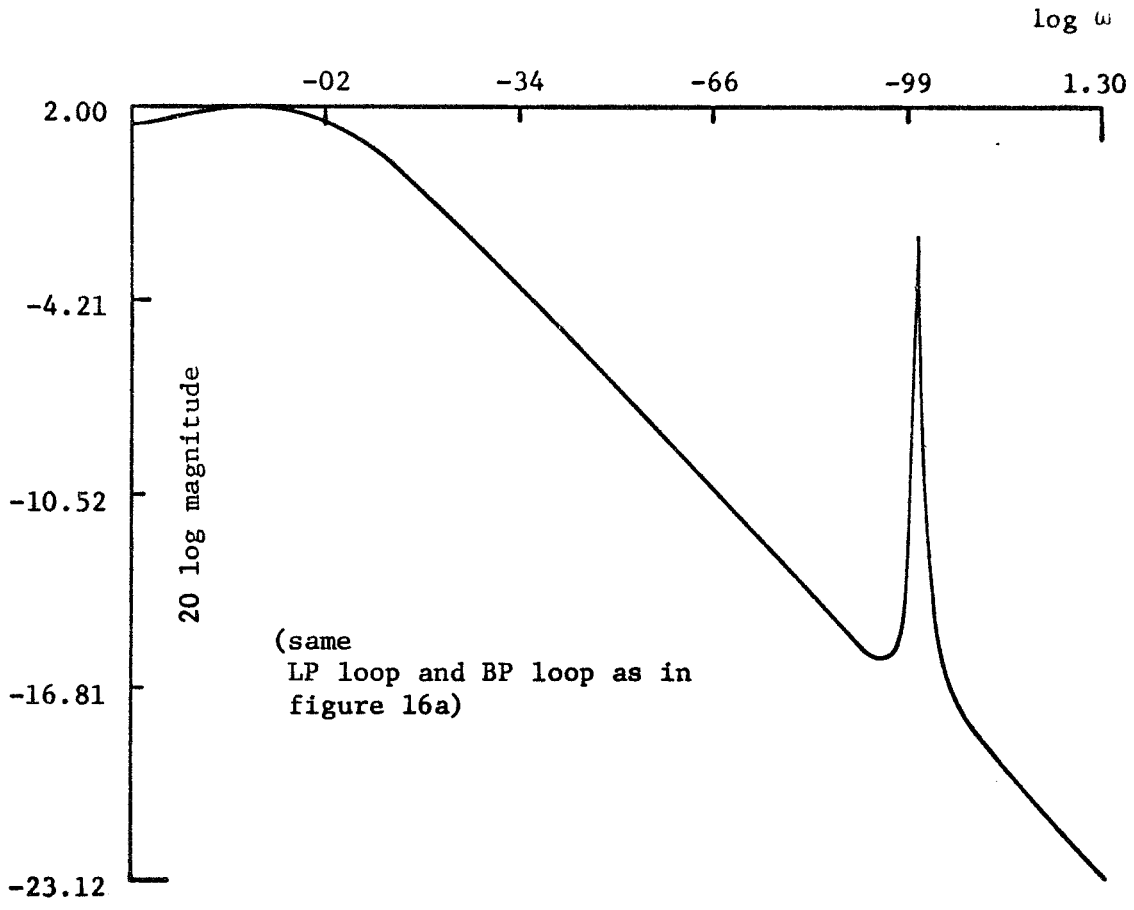

Figure 16b. L-BP M-PLL 20 Log Phase Magnitude Response for the Linear Approximation

$$K_2 = \sqrt{2} \tag{3.1.1-25}$$

and

$$a = \frac{1}{\sqrt{2}} \tag{3.1.1-26}$$

For the LP PLL portion of the M-PLL the values chosen above lead to an optimum type II LP PLL as shown in [4].

Since $$K_\delta K_V K_{f_2} = AK_2 = \sqrt{2} \tag{3.1.1-27}$$

with $$K_\delta = 1/2 \text{ unit/volt} \tag{3.1.1-28}$$

and $$K_V = 240\pi \text{ radians/unit} \tag{3.1.1-29}$$

then $$K_{f_2} = \frac{\sqrt{2}}{K_\delta K_V} = \frac{\sqrt{2}}{(1/2)\ (240\pi)} = \frac{\sqrt{2}}{120\pi} \tag{3.1.1-30}$$

and $$K_{f_1} = K_{f_2} \text{ since } AK_1 = AK_2$$

All the necessary information for solution of the state model equation (3.1.1-1) by digital computation is contained in (3.1.1-11), and (3.1.1-26). The analog computer set-up for the entire L-BP M-PLL C.M.,* shown in Figure 17, is obtained with values given by (3.1.1-21) thru (3.1.1-30).

As mentioned in section 1.1, since $F_2(s) = (1 + a/s)$ does not reject high frequency terms, an additional filter is used outside of the loop on $\tilde{e}(t)$ in order to eliminate the high harmonic components and thus to obtain the information output. The transfer function used for this LP filter is

$$F(s) = \frac{(\omega_{cc})^2}{s^2 + (\omega_{cc})\ s + (\omega_{cc})^2} \tag{2.4-1}$$

---

*C.M. is the abbreviation for carrier model.

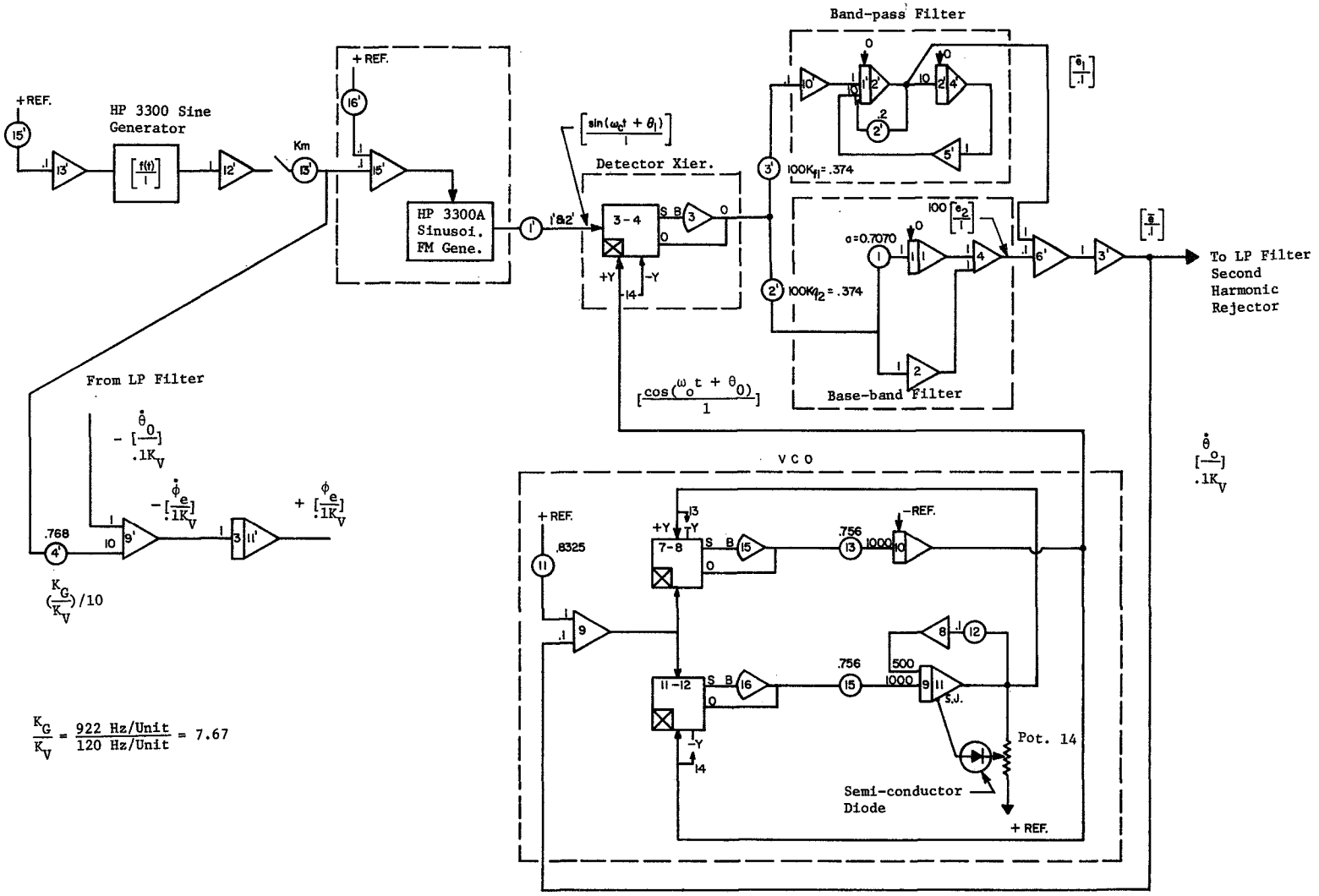

$\frac{K_G}{K_V} = \frac{922 \text{ Hz/Unit}}{120 \text{ Hz/Unit}} = 7.67$

Figure 17. M-PLL Analog Computer Simulation Set-up. $F_1(s) = (K_{f_1}s)/(s^2 + 2\zeta_{o1}\omega_{o1}s + \omega_{o1}^2)$; $F_2(s) = K_{f_2}(1 + a/s)$

where ω_{cc} is the cut-off frequency. The corresponding amplitude-frequency response of (2.4-1) is of the form shown in Figure 18.

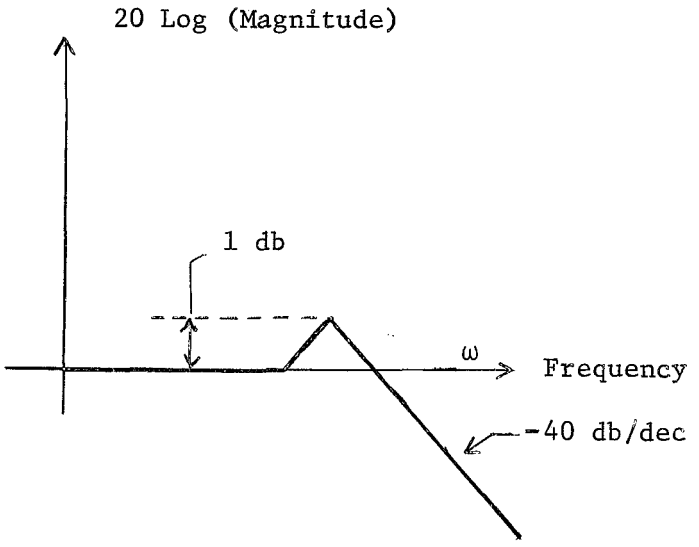

Figure 18. Amplitude-frequency Response of $\omega_{cc}^2/(s^2 + \omega_{cc}s + \omega_{cc}^2)$

From (2.4-1) we have

$$F(s) = \frac{\omega_{cc}^2 s^{-2}}{1 + \omega_{cc}s^{-1} + \omega_{cc}^2 s^{-2}} \qquad (2.4\text{-}2)$$

Applying Mason's rule for synthesis of (2.4-2) one obtains the analog computer set-up shown in Figure 19.

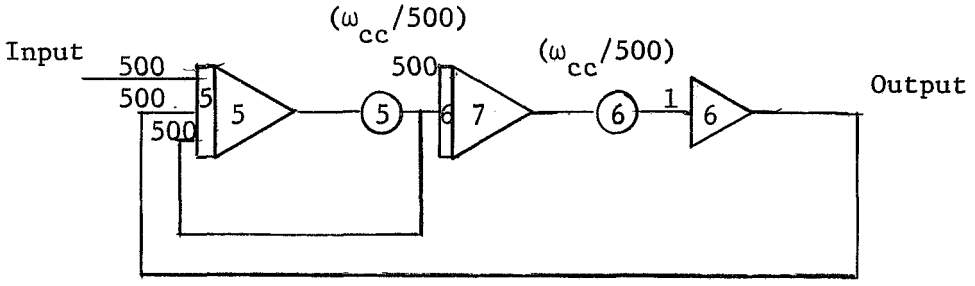

Figure 19. Low-pass Filter $\omega_{cc}^2/(s^2 + \omega_{cc}s + \omega_{cc}^2)$ Analog Computer Set-up

3.1.2 Results Of The Simulation

One of the objectives of this investigation is to evaluate the improvement of the PLL due to the band-pass filter. This improvement is measured by comparing the phase error of a low-band pass multi-filter PLL to the resulting low-pass PLL when the band-pass filter is removed from the loop.

For a LP PLL with a loop bandwidth $\omega_{n_2} = 1.0$ and $\zeta_{n_2} = 0.7070$, the closed loop gain becomes quite small at a modulating frequency of $\omega_m = 10.0$ - about 18% of the value at base-band frequencies (Figure 16). Consequently, the phase error gets so large that the characteristic phase error transition from lock PLL tracking to unlock can no longer be seen. In other words, continuous cycle skipping is not observable. The simulation shows that the oscillations of the phase error occur

around 0, $-\pi$, and $+\pi$; but not around multiples of $\pm 2\pi$.

Figures 20 a,b,c show plots of steady-state peak phase error and steady-state peak detected output vs. $\frac{\Delta\omega}{\omega_m}$ for phase error and detected output obtained by digital computation. The figures show results for both LP PLL and L-BP multi-filter PLL. One sees that for $\Delta\omega/\omega_m < .5$, the LP PLL steady-state peak detected output $e_{ss\ p}$ increases linearly with $\Delta\omega/\omega_m$. For $\Delta\omega/\omega_m$ higher it does not increase as fast as $\Delta\omega/\omega_m$ does. This coincides with the distortion present on e(t). At $\Delta\omega/\omega_m$ of about 2.2 the LP PLL detected output becomes erratic and its average peak value is independent of $\Delta\omega/\omega_m$ (unlocked PLL). This is indicated by dashed lines in Figure 20.

From Figure 20 one can see that the addition of the band-pass filter does not yield any improvement.

For frequencies higher than the individual closed-loop peak gain frequency ω_{n_1}, the L-BP PLL phase error turns out to be higher than the single low-pass PLL phase error $\phi_{e_{LP\ PLL}}$. This is because the band-pass filter introduces a net $-90°$ phase shift at higher frequencies. The effect caused by the phase shift is more clearly illustrated in Figure 21*, where steady-state peak to peak frequency error and steady-state detected output are shown as functions of the modulating frequency ω_m. Note that the maximum $e_{ss\ pp}$ does not coincide with ω_{o1}

---

* From the simulation of the M-PLL carrier model on the analog computer.

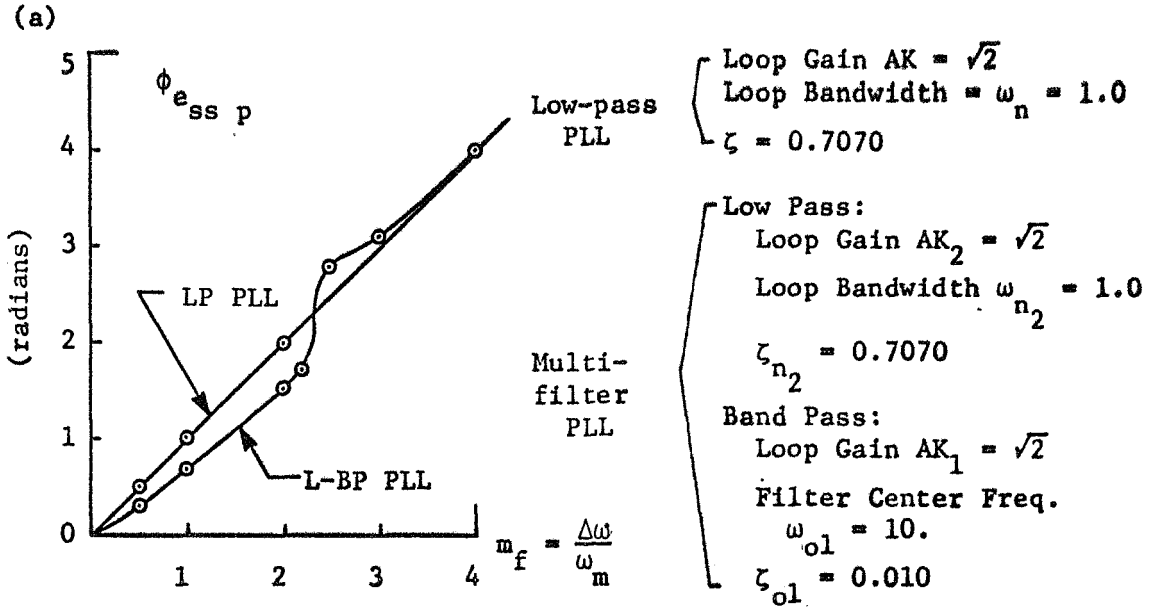

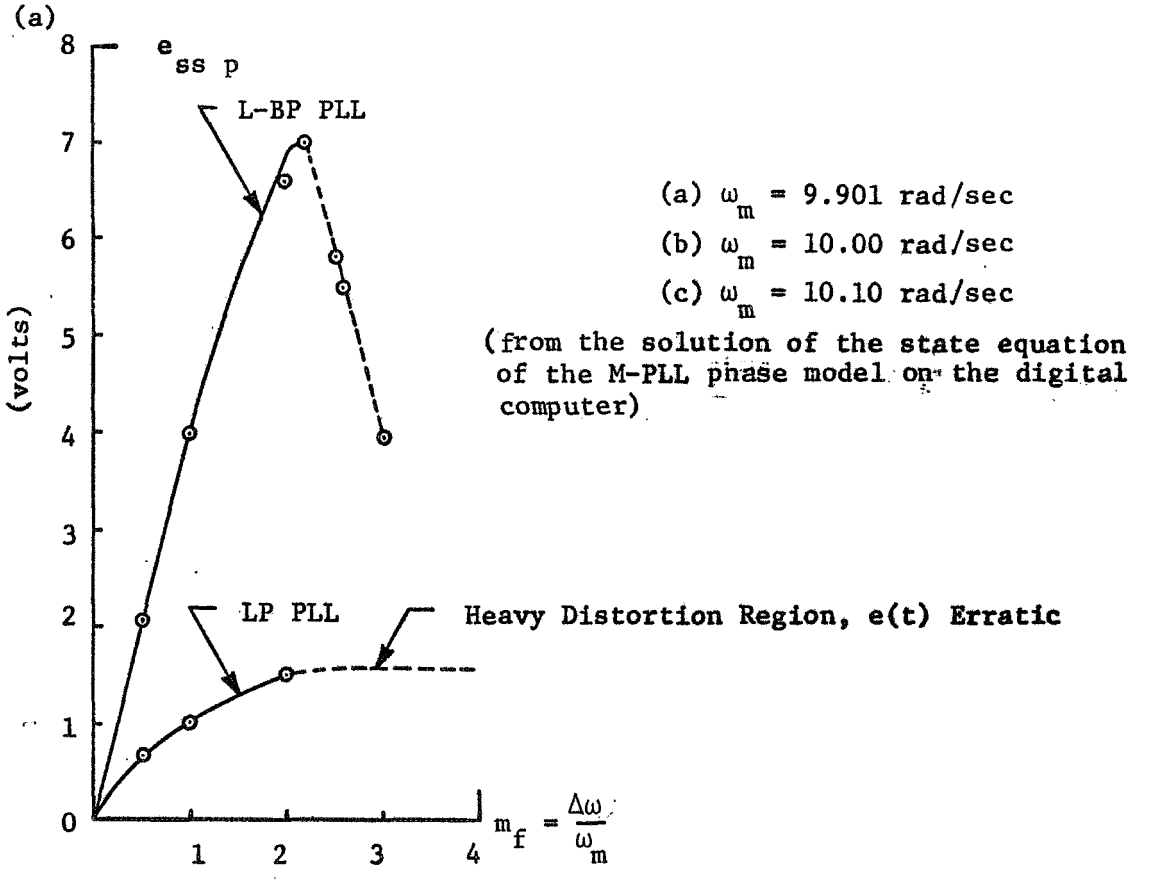

Figure 20. LP PLL and L-BP M-PLL Steady-state Peak Phase Error, and Steady-state Peak Detected Output due to Sinusoidal FM.

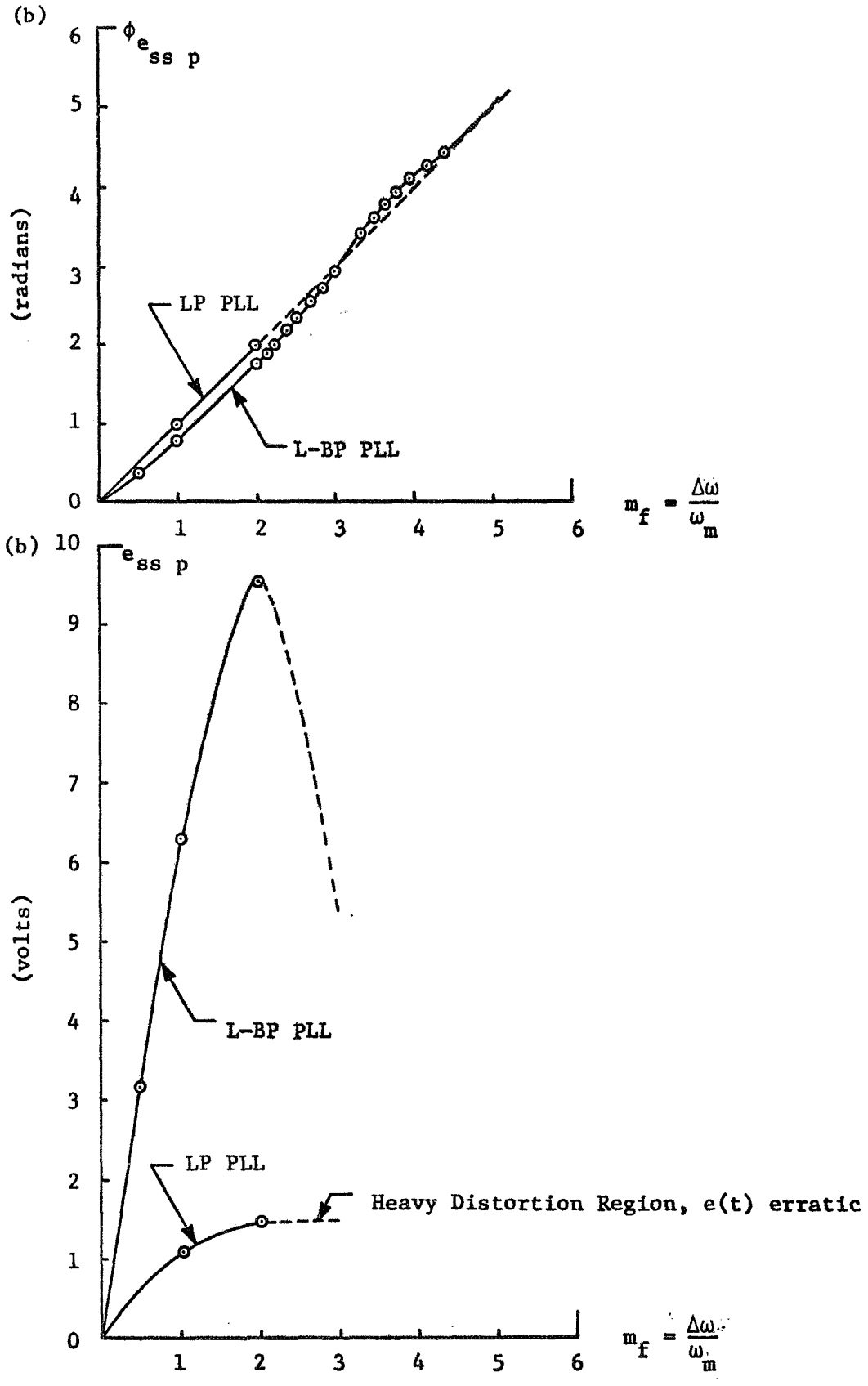
(b)
$\phi_{e_{ss\ p}}$
(radians)
LP PLL
L-BP PLL
$m_f = \frac{\Delta\omega}{\omega_m}$
(b)
$e_{ss\ p}$
(volts)
L-BP PLL
LP PLL
Heavy Distortion Region, e(t) erratic
$m_f = \frac{\Delta\omega}{\omega_m}$

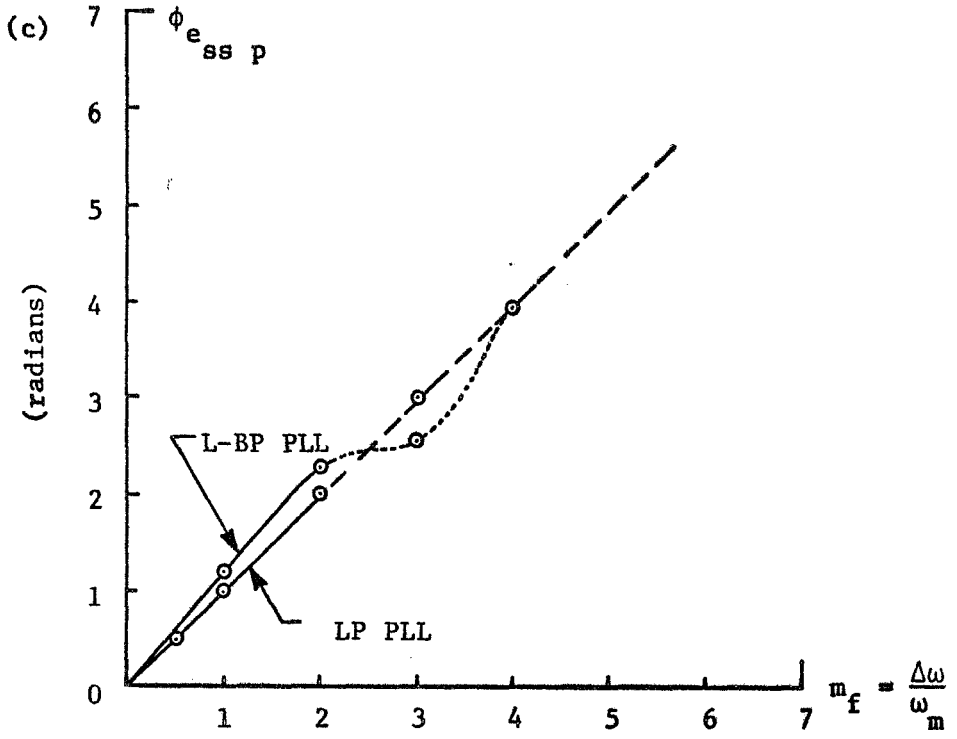
(c)
$\phi_{e_{ss\ p}}$
(radians)
L-BP PLL
LP PLL
$m_f = \frac{\Delta\omega}{\omega_m}$
0
1
2
3
4
5
6
7

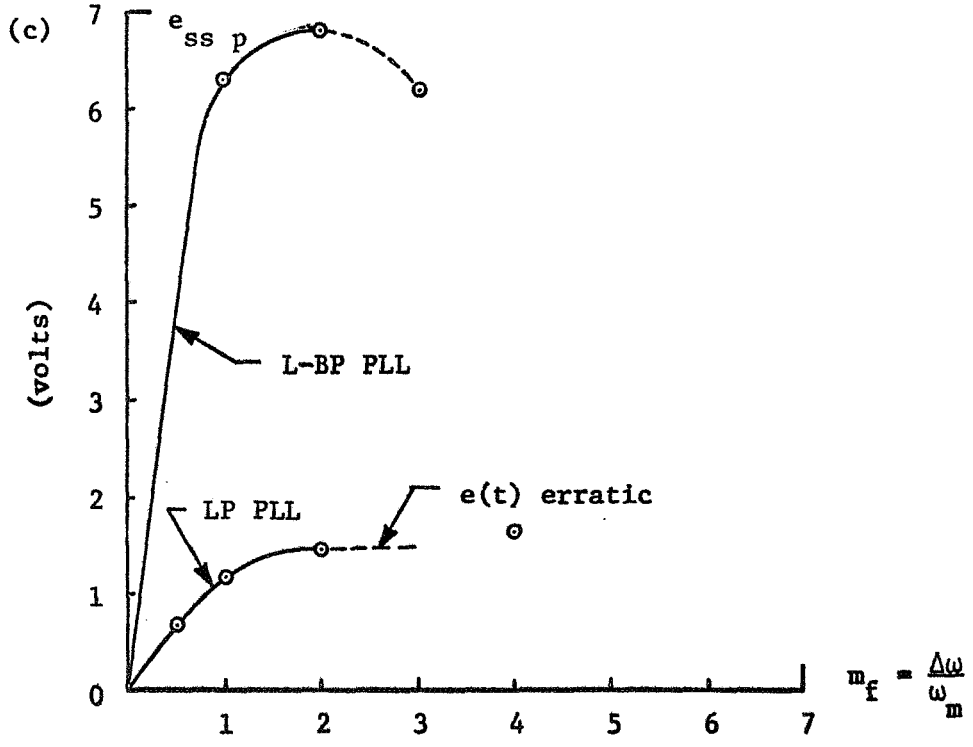
(c)
$e_{ss\ p}$
(volts)
L-BP PLL
LP PLL
e(t) erratic
$m_f = \frac{\Delta\omega}{\omega_m}$
0
1
2
3
4
5
6
7

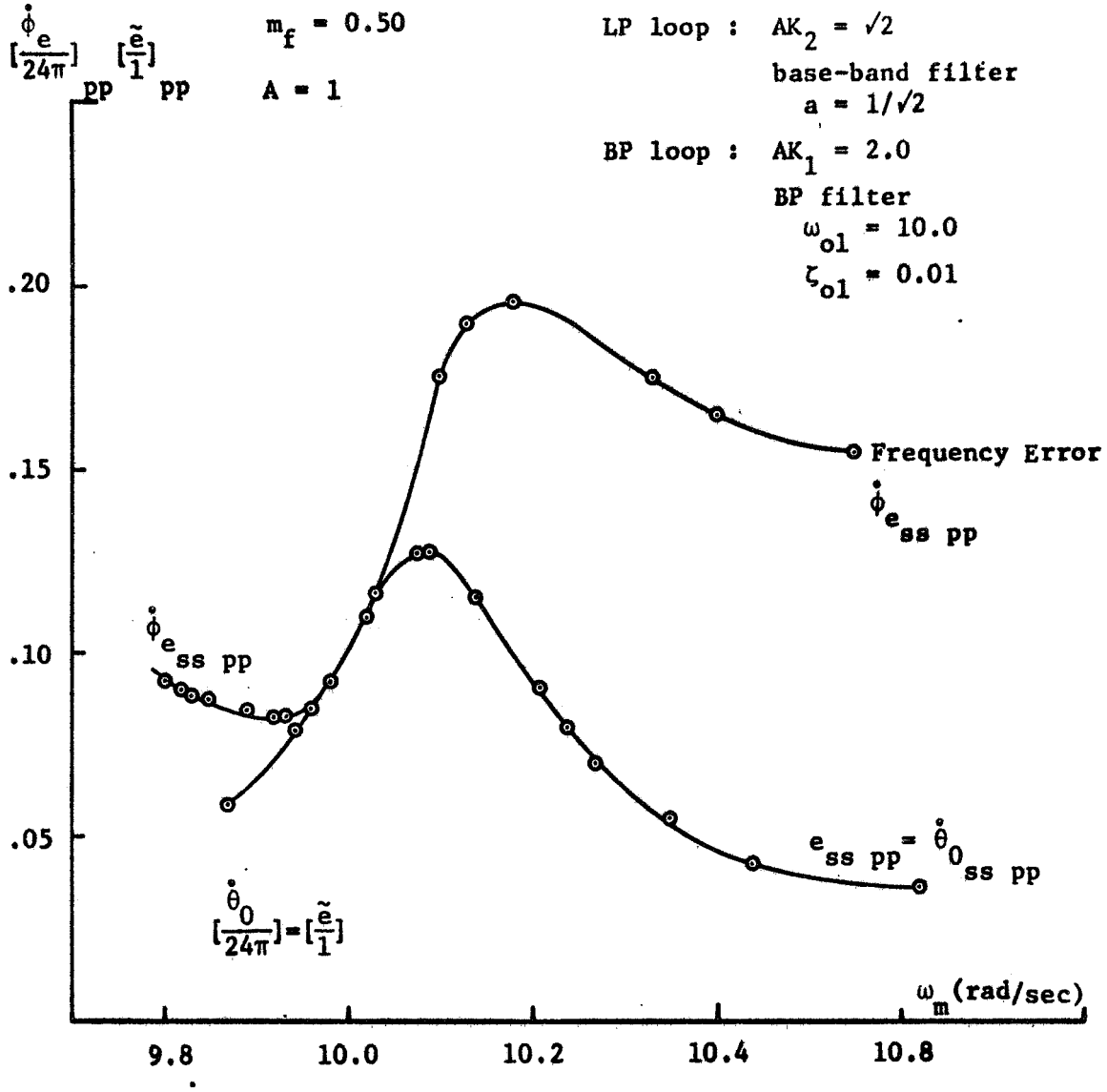

Figure 21. L-BP M-PLL Steady-state Peak to peak Frequency Error and Steady-state Peak to Peak Detected Output due to Sinusoidal FM

(from the simulation of the M-PLL C.M. on the analog computer)

3.2 A L-BP M-PLL with a Differentiator Following the BP Filter

If the -90° phase shift introduced by the band-pass used in the previous section could somehow be compensated for, then an improvement would be obtained. One solution [1] to this problem involves the addition of a differentiator following the BP filter. This section deals with the discussion of the L-BP M-PLL when a differentiator follows the band-pass filter. The same procedure illustrated in section 3.1 is followed.

The portion of the M-PLL open-loop transfer gain due to the BP filter with the differentiator becomes:

$$AK_1F_1(s)\ S\ \frac{1}{s} = \frac{AK_1 s}{s^2 + 2\zeta_{o1}\omega_{o1}s + \omega_{o1}^2} \qquad (3.2\text{-}1)$$

The root locus plot for this arrangement is shown in Figure 22.

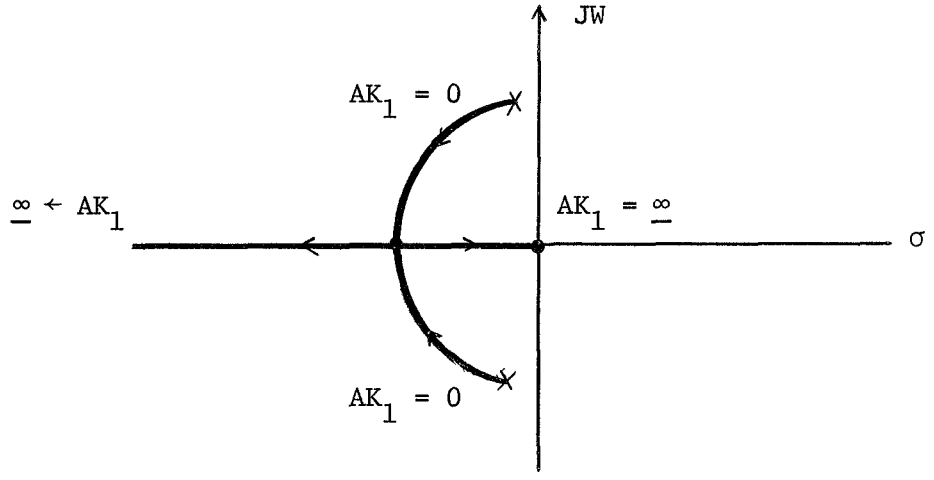

Figure 22 . Root Locus Plot for a Band-pass Filter with a Differentiator Following It.

From the root-locus plot one can see that the linear system response is stable for any value of the open-loop gain AK_1.

The corresponding BP closed-loop transfer response turns out to be

$$\frac{\theta_0(s)}{\theta_1(s)} = \frac{AK_1 \dfrac{s^2}{s^2 + 2\zeta_{o1}\omega_{o1}s + \omega_{o1}^2}}{s + AK_1 \dfrac{s^2}{s^2 + 2\zeta_{o1}\omega_{o1}s + \omega_{o1}^2}} = \frac{AK_1 s}{s^2 + 2\zeta_{o1}\omega_{o1}s + \omega_{o1}^2 + AK_1 s} \tag{3.2-2}$$

or

$$\frac{\theta_0(s)}{\theta_1(s)} = \frac{AK_1 s}{s^2 + (2\zeta_{o1}\omega_{o1} + AK_1)\, s + \omega_{o1}^2} \tag{3.2-3}$$

Of the two BP closed-loop transfer responses, namely (3.1-5) and (3.2-3), the latter gives a better BP shape. Furthermore,

$$\omega_{n_1} = \omega_{o1} \tag{3.2-4}$$

$$\zeta_{n_1} = \left(\zeta_{o1} + \frac{AK_1}{2\omega_{o1}}\right) \tag{3.2-5}$$

Note that ζ_{n_1} is a function of AK_1 and that the maximum magnitude response of (3.2-2) is less than 1.

3.2.1 Design and Simulation of the Loop

Following the same procedure illustrated in section 3.1.1 the state model equation for the L-BP M-PLL with a differentiator following

the BP filter* is found to be

$$\frac{d}{dt}\begin{bmatrix} x_1^{(1)} \\ x_2^{(1)} \\ x_1^{(2)} \\ x^{(0)} \end{bmatrix} = \begin{bmatrix} 0 & 1 & 0 & 0 \\ -\omega_{o1}^2 & -2\zeta_{o1}\omega_{o1} & 0 & 0 \\ 0 & 0 & 0 & 0 \\ -\omega_{o1}^2 & -2\zeta_{o1}\omega_{o1} & a & 0 \end{bmatrix} \begin{bmatrix} x_1^{(1)} \\ x_2^{(1)} \\ x_1^{(2)} \\ x^{(0)} \end{bmatrix} + \begin{bmatrix} 0 \\ AK_1 \sin(\theta_1 - x^{(0)}) \\ AK_2 \sin(\theta_1 - x^{(0)}) \\ (AK_1 + AK_2) \sin(\theta_1 - x^{(0)}) \end{bmatrix} \tag{3.2.1-1}$$

with the initial state vector equal to

$$\begin{bmatrix} x_1^{(1)} \\ x_2^{(1)} \\ x_1^{(2)} \\ X^{(0)} \end{bmatrix}_{t=0^+} = \begin{bmatrix} 0 \\ 0 \\ 0 \\ 0 \end{bmatrix} \tag{3.2.1-2}$$

System variables such as ϕ_e, e(t) are obtained as shown in section 3.1.1.

For the analog computer set-up, we have

$$K_{f_1} F_1(s)\ s = \frac{K_{f_1}}{1 + 2\zeta_{o1}\omega_{o1}s^{-1} + \omega_{o1}^2 s^{-2}} = \frac{\tilde{E}_1(s)}{\tilde{U}(s)} \tag{3.2.1-3}$$

---

* The band-pass filter with a differentiator following it can be considered as an equivalent BP filter of the form
$K_{f_1} s^2/(s^2 + 2\zeta_{o1}\omega_{o1}s + \omega_{o1}^2)$

Then, the analog computer set-up for (3.2.1-3) is given by

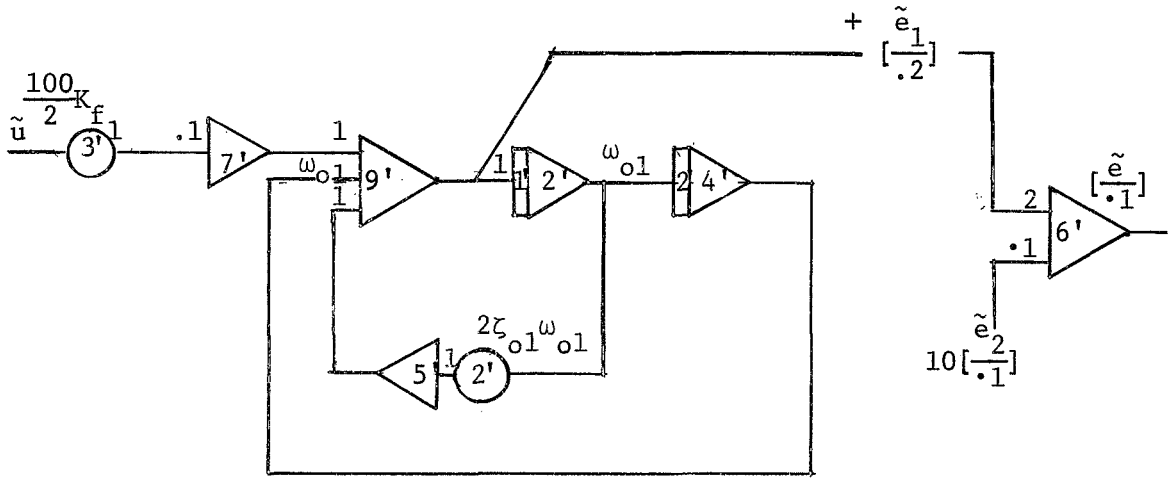

Figure 23. Analog Computer Set-up for BP Filter

$K_{f_1} s/(s^2 + 2\zeta_{o1}\omega_{o1}s + \omega_{o1}^2)$

with a Differentiator Following It

Since we use the same base-band filter as in section 3.1 the analog configuration (Figure 15) remains unaltered. We also keep the same values for ω_{n_2}, ζ_{n_2}, ω_{o1}, ζ_{o1}, and AK_2 given by (3.1.1-19) thru (3.1.1-23). Consequently,

$$K_2 = \sqrt{2} \qquad (3.2.1\text{-}4)$$

$$a = \frac{1}{\sqrt{2}} \qquad (3.2.1\text{-}5)$$

Figures 24a,b,c,d, show a linear L-BP M-PLL amplitude-frequency response for this case, when $AK_1 = 2.0$ and 13.94 respectively.

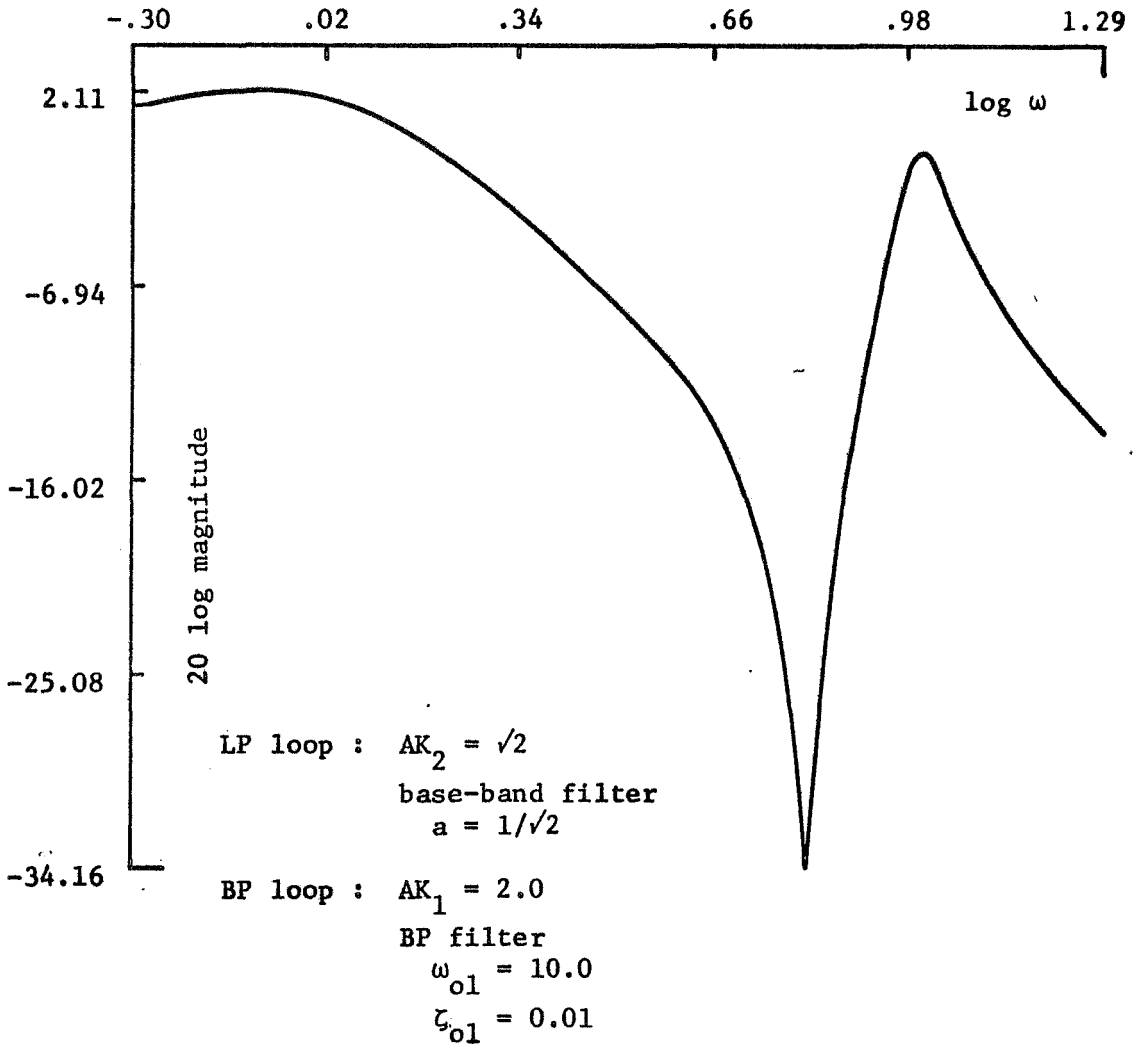

Figure 24a. Amplitude-frequency Response of a L-BP M-PLL with a Differentiator Following the BP Filter

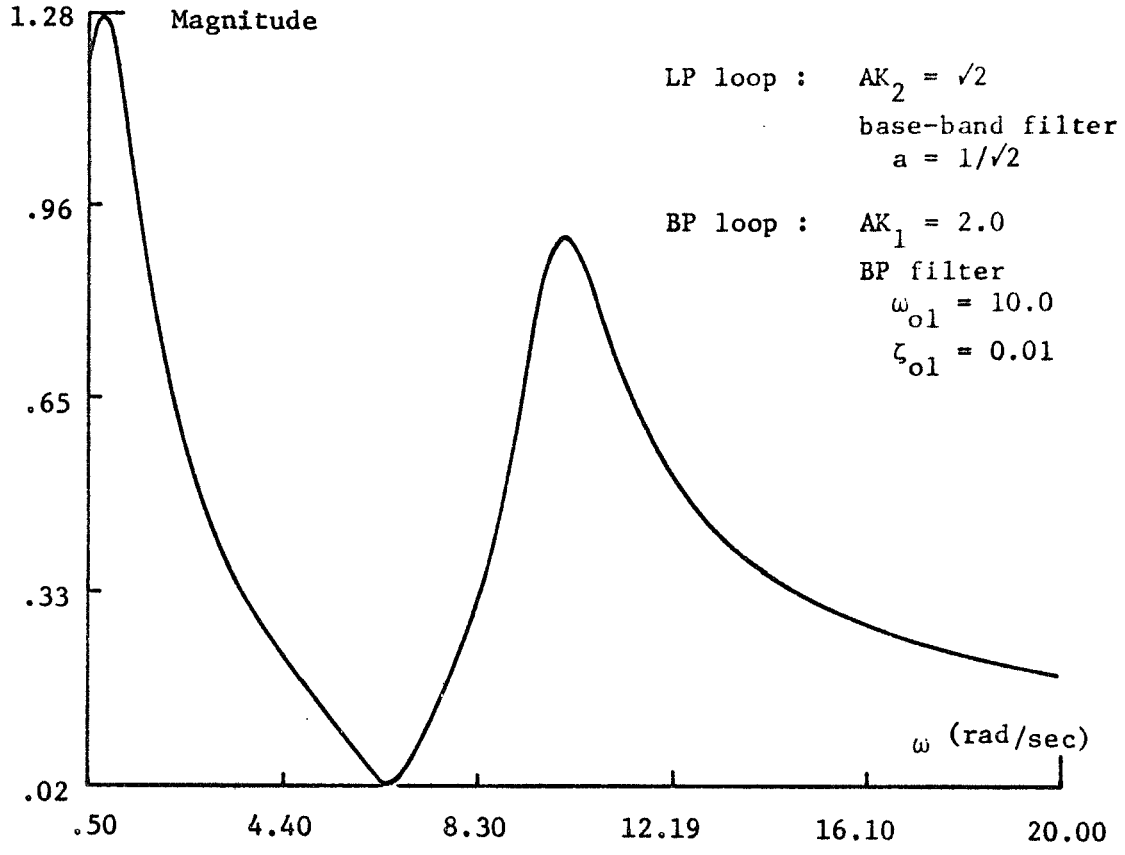

Figure 24b. Amplitude-frequency Response of a L-BP M-PLL with a Differentiator Following the BP Filter

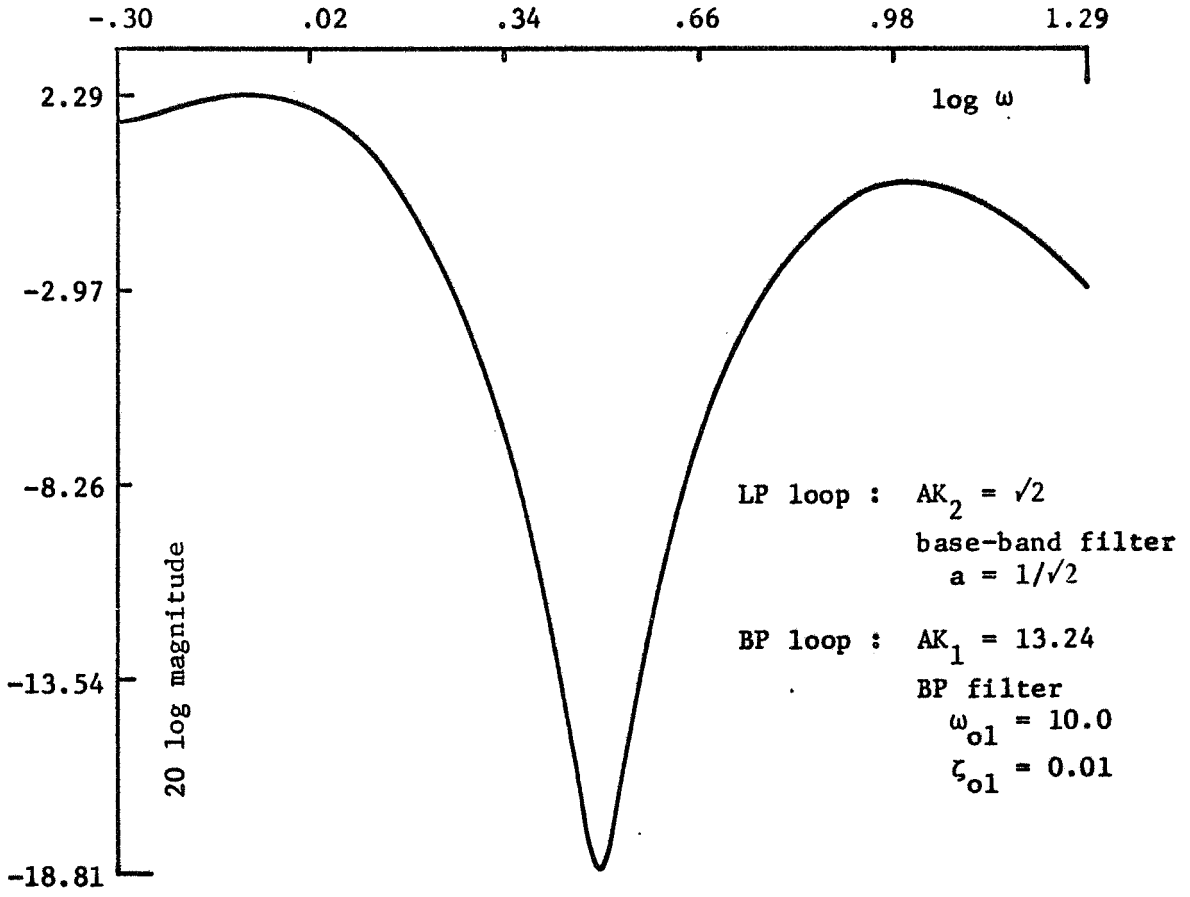

Figure 24c. Amplitude-frequency Response of a L-BP M-PLL with a Differentiator Following the BP Filter

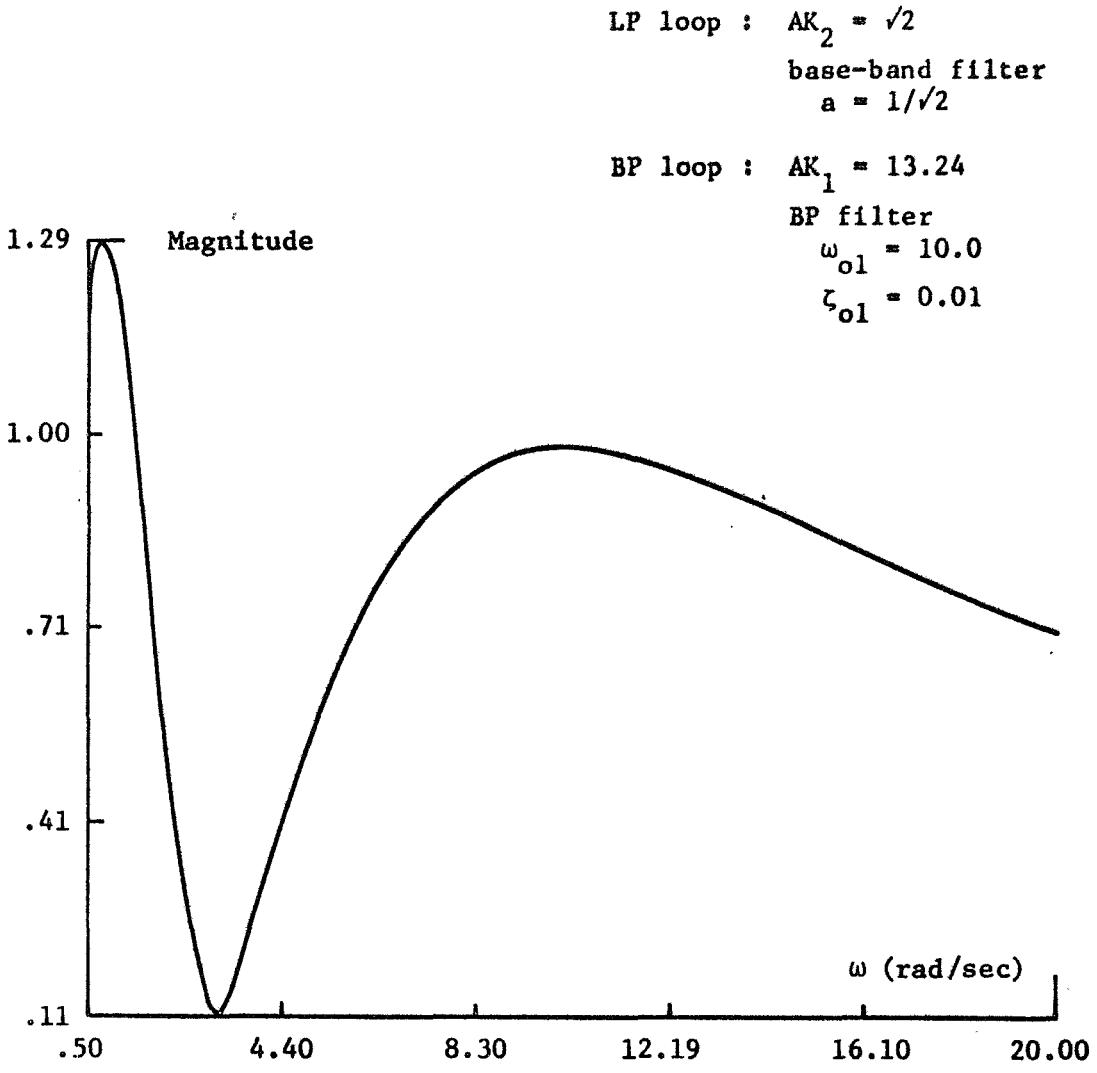

Figure 24d. Amplitude-frequency Response of a L-BP M-PLL with a Differentiator Following the BP Filter

Now, all the necessary information for solution of the state model equation (3.2.1-1) by digital computation is contained in (3.2.1-2), (3.1.1-19) thru (3.1.1-23), and (3.2.1-5).

The entire analog computer set-up for this case is obtained from Figure 17 after replacing the BP filter by that given in Figure 23. Where

$$K_{f_1} = \frac{AK_1}{K_\delta K_V} = \frac{2.0}{1/2\ 240\pi} = .264 \times (\frac{2}{100}) \qquad (3.2.1\text{-}6)$$

or

$$1/2 \cdot 100\ K_{f_1} = .264 \qquad (3.2.1\text{-}7)$$

3.22 Results of the Simulation

The results of the computer simulation show that addition of the differentiator after the band-pass filter yields significant improvement. The phase error is reduced throughout the band pass frequency range. Its minimum is at $\omega_m \cong \omega_{o1}$ and for $AK_1 = 2.01$ it is about 1/6 of the phase error obtained without the differentiator. However, the detector output is reduced by the addition of the differentiator.

Plots of peak values of frequency error, detected output, and phase error as functions of ω are shown in Figures 26 a, b.

Now for modulating frequencies near ω_{o1}, the transition from lock to unlock tracking demodulation is more clearly defined. During this transition a rapid increase in the phase error can be observed. The detected output $e(t)$ becomes smaller and erratic; therefore, θ_0 gets

smaller and, consequently, $\phi_{e\ peak} \rightarrow \frac{\Delta\omega}{\omega_m}$. Figure 25 shows a multi-filter PLL lock-unlock transition for ω_m close to ω_{ol}. As ω_m moves from ω_{ol} the transition becomes less apparent and its detection becomes more difficult.

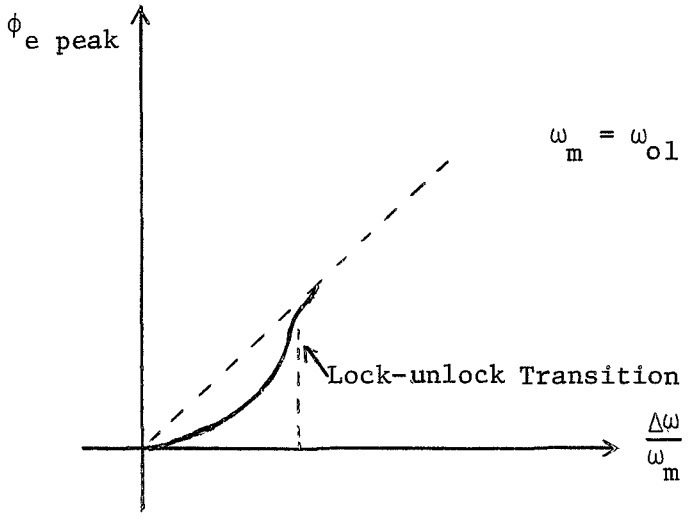

Figure 25. M-PLL Lock - unlock Tracking Transition

Plots of $\dot{\phi}_e$ vs. ϕ_e for an unlocked LP PLL for an unlocked L-BP M-PLL, and for a proper locked L-BP M-PLL with a differentiator following the BP filter are shown in Figure 26 c,d,e .

Two L-BP M-PLL lock boundary plots, determined by means of the analog computer simulation and for a single subcarrier, are shown in Figure 27 a,b . In Figure 27a, the L-BP M-PLL was first locked onto carrier plus signal (single FM subcarrier), then $\Delta\omega$ was slowly increased until the loss of lock occurred. This procedure was repeated for several values of ω_m. The procedure used to obtain Figure 27b

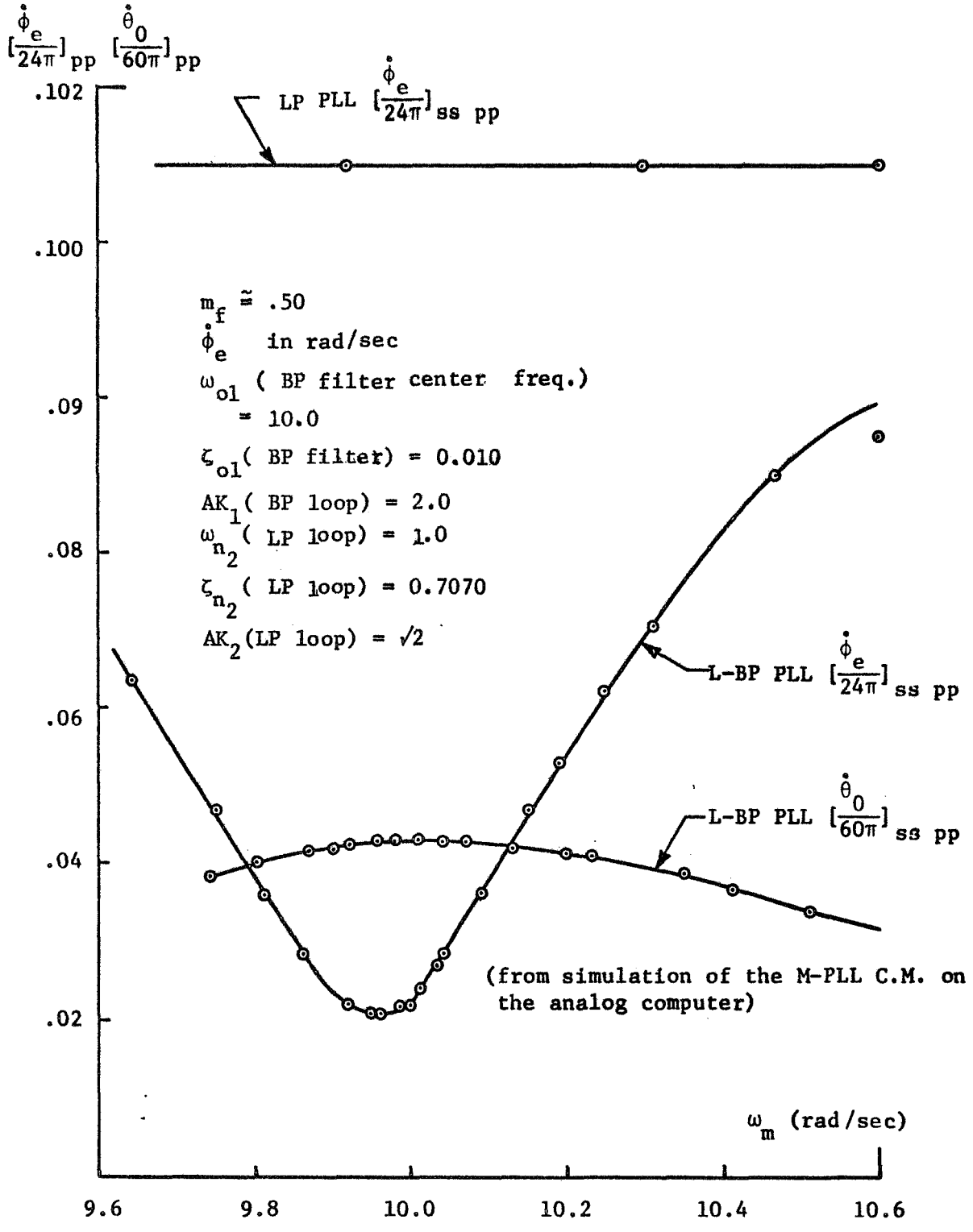

Figure 26a. L-BP M-PLL Steady-state Peak to Peak Frequency Error and Steady-state Peak to Peak Detected Output due to Sinusoidal FM with a Differentiator Following the BP Filter

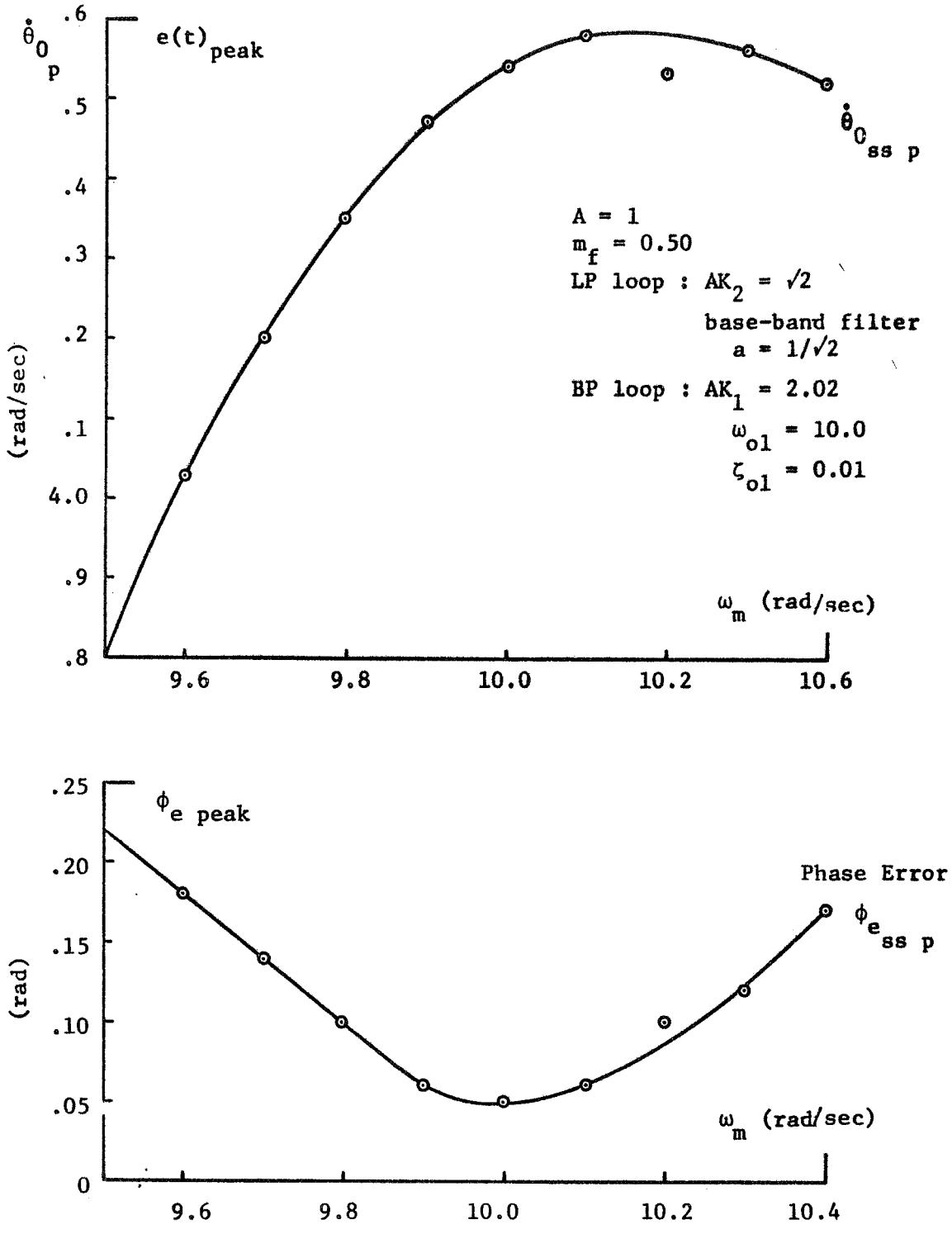

Figure 26b. L-BP M-PLL Steady-state Peak Phase Error and Steady-state Peak Detected Output due to Sinusoidal FM with a Differentiator Following the BP Filter. (from the solution of the state equation of the M-PLL phase model on the digital computer)

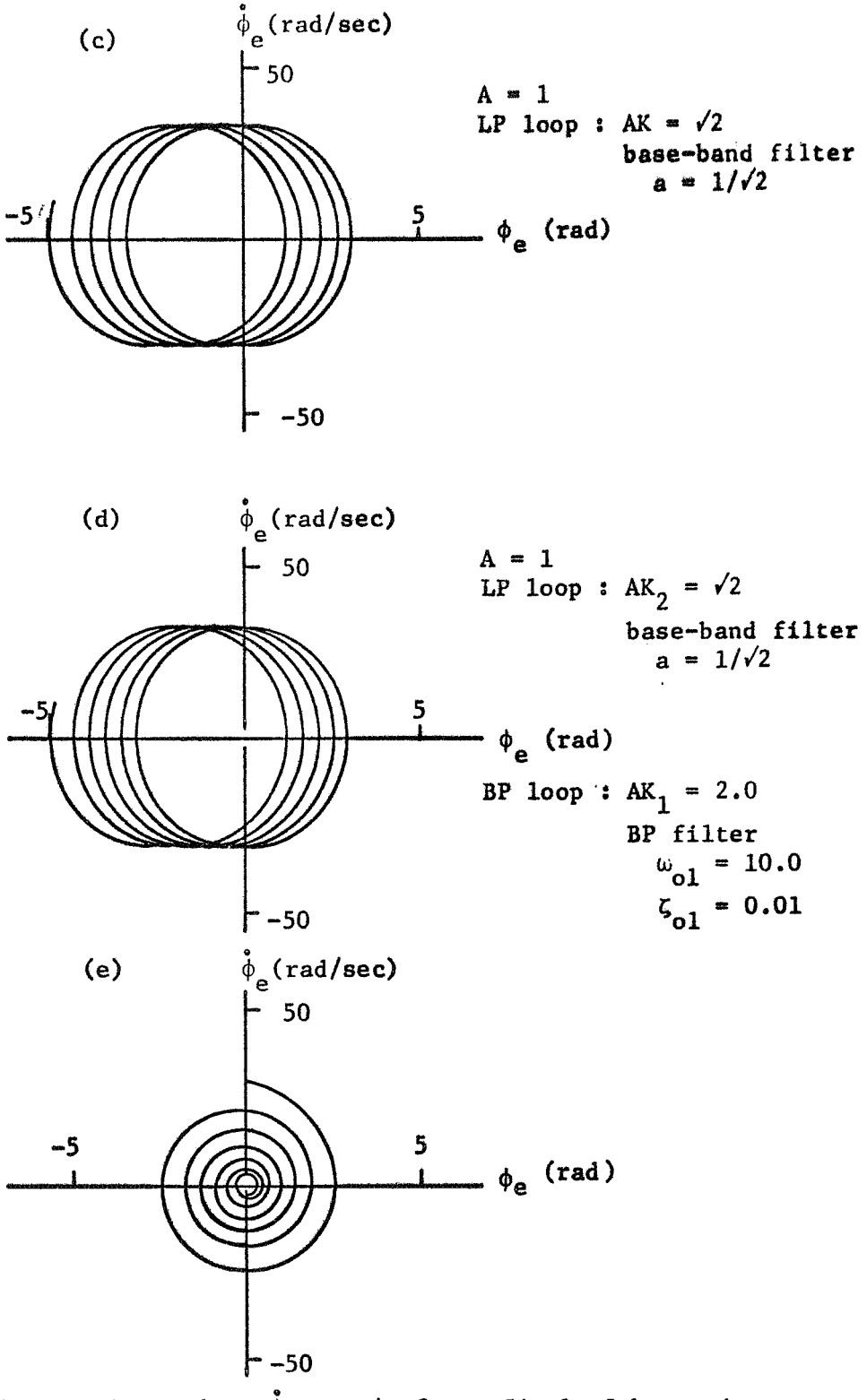

Figure 26 c,d,e. Phase-plane $\dot{\phi}_e$ vs. ϕ_e for a Single Sub-carrier

c) Unlocked L-PLL d) Unlocked L-BP M-PLL
e) Locked L-BP M-PLL with a Differentiator Following the BP Filter

(from simulation of the M-PLL Ph.M. on the analog computer)

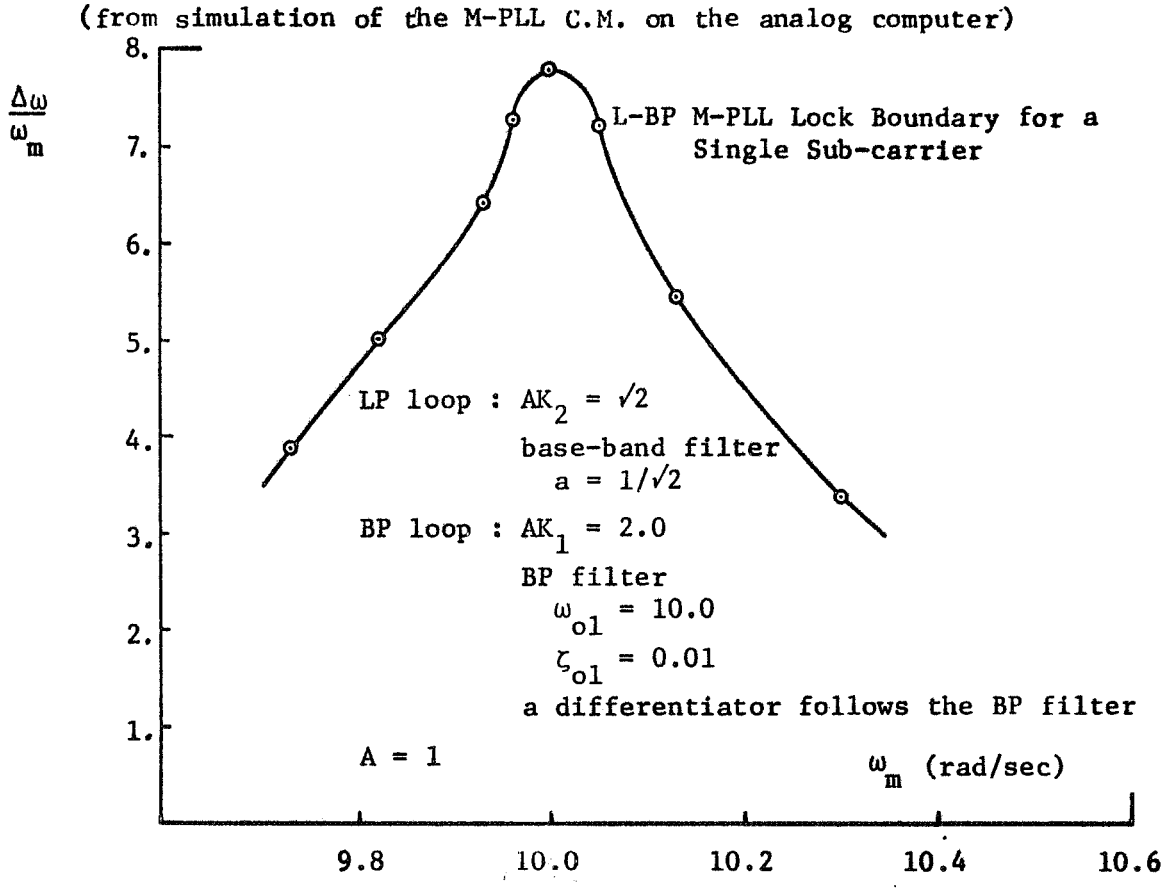
(from simulation of the M-PLL C.M. on the analog computer)
$\frac{\Delta\omega}{\omega_m}$
8.
7.
6.
5.
4.
3.
2.
1.
L-BP M-PLL Lock Boundary for a Single Sub-carrier
LP loop : $AK_2 = \sqrt{2}$
base-band filter
$a = 1/\sqrt{2}$
BP loop : $AK_1 = 2.0$
BP filter
$\omega_{o1} = 10.0$
$\zeta_{o1} = 0.01$
a differentiator follows the BP filter
A = 1
ω_m (rad/sec)
9.8
10.0
10.2
10.4
10.6

Figure 27a.

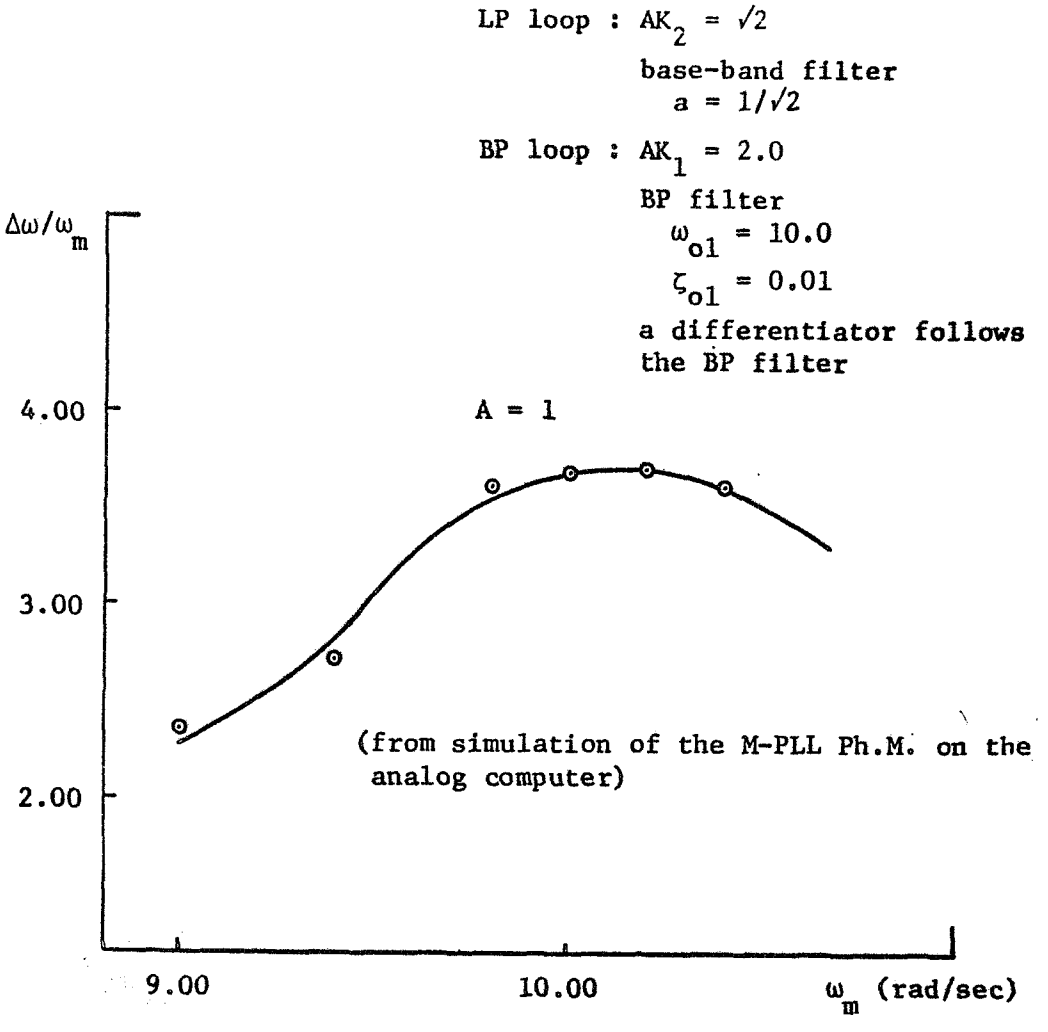

Figure 27b. L-BP M-PLL Lock-boundary when the FM Single Sub-carrier is Applied at $t=0^+$

was different from that used for Figure 27a. For Figure 27b the modulating signal was applied at $t = 0^+$ having set the value of $\Delta\omega$ beforehand. If the L-BP M-PLL resulted locked-in, then $\Delta\omega$ was increased. If the L-BP M-PLL resulted un-locked, then $\Delta\omega$ was decreased. This operation was repeated until a suitable value for the lock boundary point was obtained. Different values of ω_m were investigated.

CHAPTER IV
CONCLUSION

4.1 Summary

The carrier model and the phase model for the generalized multi-filter PLL are considered, and state equations for the phase model are derived. The state equations for the carrier model can be obtained in an analogous manner. Analog computer configurations showing direct component interconnections for simulation of both carrier and phase multi-filter PLL are derived, and problems encountered with the implementation of these configurations are considered.

Simulations of a low-band pass multi-filter PLL, for the case of sinusoidal FM with a single deterministic sub-carrier, were performed to investigate the improvement of the LP PLL due to the band-pass filter. This improvement is measured by comparing the phase error of the L-BP multi-filter PLL with the resulting PLL when the band-pass filter is removed from the loop. The particular loop considered has a base-band filter $(1 + a/s)$ in parallel with an active tuned-loop filter of the form $K_{f_1} s/(s^2 + 2\zeta_{o1}\omega_{o1}s + \omega_{o1}^2)$. The modulating frequency ω_m is taken approximately 10 times the individual low-pass loop bandwidth ω_{n_2}. The loop-gain due only to the base-band filter is small, and consequently the error is high.

The simulation is accomplished by solution of the state equation for the phase model on a CDC 3300 digital computer, using the Adams-Mouton numerical integration technique, and by simulation of the carrier model showing direct component interconnection on two EAI TR-20 analog computers.

Computer results show that the steady-state peak L-BP multi-filter PLL phase error ($\phi_{e_{\text{L-BP PLL}}}$) is smaller than the steady-state peak LP PLL phase error ($\phi_{e_{\text{LP PLL}}}$) for frequencies smaller than the band-pass loop center frequency ω_{n_1} and larger for higher frequencies. The fluctuation in the error function is comparatively insignificant; therefore, the transition between lock to unlock tracking is difficult to observe. The relative increase of the steady-state peak $\phi_{e_{\text{L-BP PLL}}}$ with respect to the steady-state peak $\phi_{e_{\text{LP PLL}}}$ can be explained in terms of the net -90° phase shift introduced by the band-pass filter. The result shows that the maximum steady-state peak occurs at the band-pass loop center frequency ω_{n_1} which is higher than the band-pass filter center frequency ω_{o1} by an amount approximately equal to the individual band-pass loop gain AK_1.

The negative phase shift is compensated for by the addition of a differentiator following the band-pass filter. This leads to a sharp decrease in the steady-state peak $\phi_{e_{\text{L-BP PLL}}}$ about its minimum which occurs at $\omega_m = \omega_{n_1}$. In turn, the individual band-pass loop center frequency ω_{n_1} is also equal to the band-pass filter center frequency ω_{o1}. For values of ω_m close to ω_{n_2}, the transition between lock and unlock tracking is more clearly defined.

4.2 Suggestion For Further Studies

Signal fidelity is proportionally related to the loop filter bandwidth of the FM discriminator used for its detection , while the signal to noise ratio is inversely related to it. Namely, for a minimum

of modulation distortion it is desirable to have a large value for the loop filter bandwidth BW. Conversely for a large signal to noise ratio it is necessary that the BW be small. Since in many practical applications it is useful to exchange signal fidelity for small BW, it is necessary to know the minimum BW for which the system is still in lock.

It would be worthwhile to obtain boundary lock regions for the bandwidth as a function of modulation indices and frequencies ω_m.

The work in this thesis involves the use of a single sinusoidal deterministic FM sub-carrier. A subsequent study should be performed considering the use of many sub-carrier inputs.

For a more complete study the effect of noise should also be considered.

CHAPTER V

BIBLIOGRAPHY

(a) References Cited

[1] Liccini, R. P., "FM Signal Data Demodulation System Analysis", TRW System, Monthly Progress Report, January 31, 1968.

[2] Viterbi, A. J., Principles of Coherent Communications, McGraw-Hill Book Company, New York, 1966.

[3] Corl, Louis, "A Phase-lock Loop Simulation and Its Behavior at Low Carrier to Noise Ratios", New Mexico State University, E.E. Master of Science Thesis, Las Cruces, New Mexico, 1969.

[4] Hintz, Thomas, "A Digital Simulation Study of a Phase-lock Loop Demodulator", New Mexico State University, E.E. Master of Science Thesis, Las Cruces, New Mexico, 1968.

(b) Other References

[1] F. Carden, L. Kelly, and T. Hintz, "The FDM Demodulating Characteristics of Nonlinear Phase-lock Loops", NTC-68 Record, Houston, Texas.

[2] Gardener, Floyd M., Phaselock Techniques, John Wiley and Sons, Inc., New York, 1966.

[3] Panter, Philip F., Modulation, Noise and Spectral Analysis,McGraw-Hill Book Company, New York, 1965.

[4] Koenig, Tokad, Kesovan, Analysis of Discrete Physical Systems, McGraw-Hill Book Company, New York, 1967.

[5] Ogata, Katsuhiko, State Space Analysis of Control Systems, Prentice-Hall, Inc., New York, 1967.

[6] Pousson, J. R. and R. P. Liccini, "Preliminary Design Report for Modification of the FM Demodulator of the Signal...", TRW System Report No. 05952-6218-R0-00, June 24, 1968.